ORNL/TM-2001/109

OAK RIDGE
NATIONAL LABORATORY
MANAGED BY UT-BATTELLE
FOR THE DEPARTMENT OF ENERGY

Phase Equilibrium Studies of Savannah River Tanks and Feed Streams for the Salt Waste Processing Facility

C. F. Weber

UT-BATTELLE
ORNL-27 (4-00)

ORNL/TM-2001/109

Computational Physics and Engineering Division (10)

Phase Equilibrium Studies of Savannah River Tanks and Feed Streams for the Salt Waste Processing Facility

C. F. Weber

Date Published: June 2001

Prepared by the
OAK RIDGE NATIONAL LABORATORY
P.O. Box 2008
Oak Ridge, Tennessee 37831-6370
managed by
UT-BATTELLE, LLC
for the
U.S. DEPARTMENT OF ENERGY
under contract DE-AC05-00OR22725

CONTENTS

LIST OF FIGURES

LIST OF FIGURES (continued)

LIST OF TABLES

ABSTRACT

A chemical equilibrium model is developed and used to evaluate supersaturation of tanks and proposed feed streams to the Salt Waste Processing Facility. The model uses Pitzer's model for activity coefficients and is validated by comparison with a variety of thermodynamic data. The model assesses the supersaturation of 13 tanks at the Savannah River Site (SRS), indicating that small amounts of gibbsite and or aluminosilicate may form. The model is also used to evaluate proposed feed streams to the Salt Waste Processing Facility for 13 years of operation. Results indicate that dilutions using 3–4 *M* NaOH (about 0.3–0.4 L caustic per kg feed solution) should avoid precipitation and reduce the Na^+ ion concentration to 5.6 *M*.

1. INTRODUCTION

Much experience has shown that some simulants of wastes at the Savannah River Site (SRS) form supersaturated solutions of metastable compounds and slowly reach thermodynamic equilibrium, a state that can be predicted by numerical modeling. It is possible that SRS wastes being fed to the Alpha Sorption system will also be supersaturated or become supersaturated upon dilution to 5.6 *M* Na. Post-filtration precipitation of solids could be a serious problem for Cs removal using Solvent Extraction. Hence, SRS will require a tool (i.e., model) to determine if the SRS wastes are supersaturated and, if so, the quantity of NaOH to add in the dilution step to prevent precipitation.

Based on initial modeling efforts at Oak Ridge National Laboratory (ORNL), it has been previously suggested that dilutions be performed with sufficient NaOH to prevent precipitation. A sample calculation was provided by ORNL showing the quantity of NaOH required for SRS average salt simulant to prevent precipitation when diluted from 6.4 *M* to 5.6 *M*. This calculation was used to estimate the amount of NaOH that would have to be added to the incoming waste in SRS's material balances for the Bases, Assumptions, and Results report (BAR).

Researchers at ORNL have continued to develop a capability for modeling the phase equilibrium behavior of concentrated waste solutions.[1-2] Recently this work has focused on various problems at Hanford and Savannah River, including pipe plugging, the SRS evaporators, and possible precipitations in crystalline silico-titanate (CST) material. In examining these issues, calculational methodology has been perfected and a sizable database has been developed. The primary purposes of this work are (1) to evaluate the accuracy of the ORNL computer model, (2) determine the equilibrium state of waste in SRS tanks with respect to crystallization of solids, and (3) measure the impact of diluting radioactive waste with NaOH solution. This study represents formal documentation of the work outlined in technical task request HLW-SDT-TTR-99-37.2 and addressed in technical task plan ORNL/CF-99/65.

2. VALIDATION OF THE MODEL

The ORNL model calculates phase equilibrium by minimization of total Gibbs energy of the entire chemical system. The method is based on the code SOLGASMIX, which is described elsewhere in detail.[3,4] Necessary input parameters are the Gibbs Energy of Formation ΔG° for each species, and activity coefficient parameters for aqueous species. These are required at whatever temperature the calculation will be performed. The Pitzer procedure is used to calculate activity coefficients, requiring binary parameters $\beta^{(0)}$, $\beta^{(1)}$, and C for each cation-anion pair. In addition, accurate solubility predictions usually require mixture parameters θ (between ions of like charge), ψ (involving three ions, not all with same charge), and λ (interactions of ions with neutral species). The details of Pitzer's model can be found in refs. 5 and 6.

A fairly extensive database has been developed over the course of many studies on sludge and simulant processing. The input parameters can be expressed as empirical functions of temperature:

$$\frac{\Delta G^\circ}{RT} = A + B\left(T - T_0\right) + C\left(\frac{1}{T_0} - \frac{1}{T}\right) + D\ \ln\left(T / T_0\right) + E\left(T^2 - T_0^2\right) \quad , \qquad (1)$$

where T_0 = 298.15 K. From Eq. (1), it is seen that the coefficient A represents the parameter value at 25°C. With sufficient data, one or more temperature coefficients can also be determined by nonlinear regression. The parameters used to model SRS wastes and simulants are given in Appendix A. Many of these parameters have been verified and documented previously, and references are provided. Validation of aluminosilicate systems is described in the following subsections. We first describe Al and Si systems separately and then the combination of the two.

2.1. Na-Al-OH

Model parameters are taken from the review by Wesolowski.[7] He regards highly the data of Russell et al.[8] for solubility of gibbsite; hence, these latter data are used to validate model calculations. The two are compared in Fig. 1, where it is seen that the model matches data closely at all three temperatures.

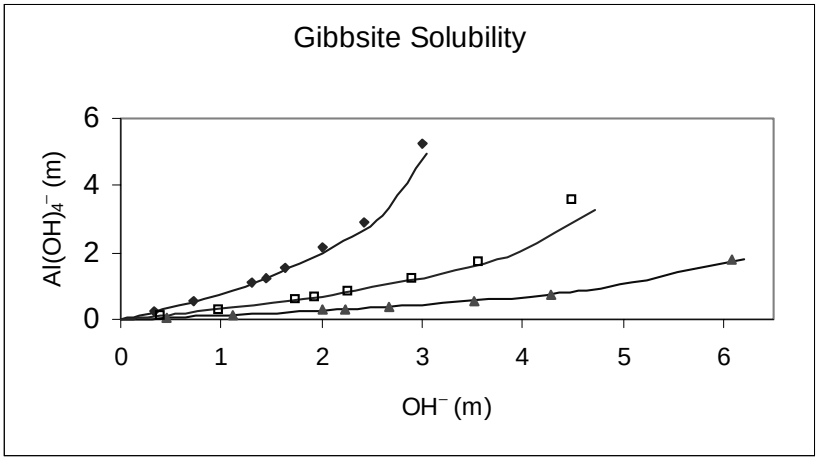

Fig. 1. Gibbsite solubility in NaOH solutions. Data from ref. 8: △ 40°, □ 70°, ♦ 100°C. — Calculations.

2.2. Na-Si-OH

This system has recently been extended to high temperatures (above 100 °C) in support of the SRS Evaporator programs.[9] While this study is concerned more with lower temperatures in the range 20–80 °C, it is important that the model be consistent. Hence, the model was developed with the entire range 20–120 °C in mind.

2.3. Silicate Hydrolysis, Polymerization, Ionization

Upon dissolution in aqueous solutions, solid silica hydrolyzes to form monomeric silicic acid:

$$SiO_2 + 2H_2O \leftrightarrow Si(OH)_4 \quad (2)$$

Dimerization joins two silicon atoms through a common bond with an oxygen atom and releases one water molecule:

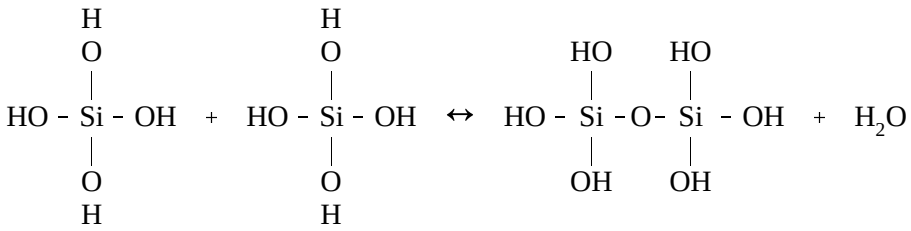

(3)

Additional polymerization occurs through analogous bonding of multiple OH groups which form chains, rings, or three-dimensional structures. Many of these shapes have been identified through NMR spectroscopy and other techniques. The hydroxyl groups can also form silicate anions, as shown for the monomer below:

$$\mathrm{Si(OH)_4} \leftrightarrow \mathrm{H^+} + \mathrm{SiO(OH)_3^-} \tag{4a}$$

$$\mathrm{SiO(OH)_3^-} \leftrightarrow \mathrm{H^+} + \mathrm{SiO_2(OH)_2^{2-}} \tag{4b}$$

As alkalinity increases, ionization also increases. To simplify terminology, the notation from ref. 10 was adopted to represent polymeric species:

$$(i, j) = \mathrm{Si}_j\mathrm{O}_m(\mathrm{OH})_n^{i-} \tag{5}$$

where *m* and *n* vary according to the bonding arrangements of the various species. Several common examples are shown in Table 1.

Each of the examples in Table 1 is symmetric, however, this need not be the case. The processes of dissolution, polymerization, and ionization create a tremendously complicated system in which hundreds of individual species may exist. Modeling such a system requires simplification, empiricism, and even heuristic reasoning. Furthermore, it is important to integrate silicate behavior with other electrolyte components, which are modeled using Pitzer's ion interaction treatment.

Table 1. Common silicate polymers

Name	Formula[a]	Structure[b]
Dimer	$[Si_2O_{1+n}(OH)_{6-n}]^{n-}$	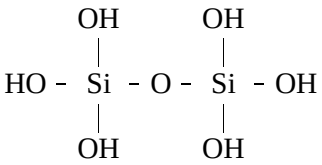
Linear trimer	$[Si_3O_{2+n}(OH)_{8-n}]^{n-}$	Si —Si —Si
Linear tetramer	$[Si_4O_{3+n}(OH)_{10-n}]^{n-}$	Si —Si —Si —Si
Cyclic trimer	$[Si_3O_{3+n}(OH)_{6-n}]^{n-}$	
Cyclic tetramer	$[Si_4O_{4+n}(OH)_{8-n}]^{n-}$	
Prismatic hexamer	$[Si_6O_{9+n}(OH)_{6-n}]^{n-}$	
Prismatic octamer	$[Si_8O_{12+n}(OH)_{8-n}]^{n-}$	
Generic polymer	$(SiO_2)_j$	

[a] n = 0, 1, 2, ...

[b] Except for dimer, all oxygen linkages are denoted by lines. If not shown, silicon atoms occur at vertices. OH and O^- groups are not shown except for dimer.

As seen from the examples in Table 1, each silicon atom is connected via an oxygen bridge to as many as four other silicon atoms. Each silicon atom is classified according to its "connectivity type," the number of other silicon atoms to which it is connected in the molecule. NMR measurements generally determine the presence of these different connectivity types, labeled Q^0, Q^1, Q^2, Q^3, and Q^4. For example, Q^0 represents the total inventory of species in which no silicon atom is adjacent to another (monomeric species). The dimer and end groups of other linear molecules comprise the Q^1 group, since each is connected to exactly one other silicon atom. The group Q^4 represents large polymers in which virtually every silicon atom connects to another; this

could also represent precipitated amorphous silica. Interior atoms of linear molecules and the cyclic species correspond to Q^2, where each silicon atom is connected to two others. However, the sharp bond angles in the cyclic trimer produce a separate NMR signal, which is denoted as Q^2_Δ. Analogously, the groups Q^3 and Q^3_Δ correspond to connectivities with three other silicon atoms, such as those in the prismatic octamer and hexamer, respectively. Sometimes it is possible for the NMR signal to distinguish other minor differences within connectivity groups. However, such determinations are highly uncertain and contribute little to model capabilities. Therefore, this study was only concerned with the following basic connectivity groups: Q^0, Q^1, Q^2, Q^2_Δ, Q^3, Q^3_Δ, and Q^4 as represented by the regular structures in Table 1. Data are appropriated from Svensson et al.[10] and McCormick et al.[11] at 25 °C, and from Kinrade and Swaddle[12] in the range 0 –100 °C.

2.4. Solubilities

Silicic acid is sparingly soluble near neutral pH, and this is affected slightly by the presence of other ions. These effects were measured for many common salt solutions,[13–16] and some of the results are listed in Table 2. This effect can be incorporated into the Pitzer model through the coefficients λ_{ij}, which describe interactions between ions and neutral species.

Many researchers have measured silicate solubility in caustic solutions at or near 25 °C; these results are summarized by Eikenberg.[17] Zarubin and Nemkina[16] give solubilities at 25 °C in 1 *M* and 3 *M* NaCl solutions as a function of pH; however, there is a lack of data in solutions of both NaOH and $NaNO_3$, or in caustic solutions at higher temperatures. We are in the process of making such measurements.

Table 2. Experimental values on the amorphous silica solubilities

Reference	Type of data	pH range	Data points	max I (m)
15	Solubility in NaOH	8 - 10.7	12	0.1
16	Solubility in NaOH + 1 *M* NaCl	9 - 10.7	18	1
	+ 3 *M* NaCl	8.8 - 10.3	14	3
14	Solubility in NaCl	~7	12	6.14
	in KNO_3	~7	12	3.76
	in KCl	~7	12	4.81
13	Solubility in $NaNO_3$	~7	9	6.12

2.5. Modeling Silicate Species

The most common approach to modeling silicate species in high caustic solutions is to select several species as representative samples and to estimate empirical formation constants. One study assumed only the monomer and the dimer, but it allowed all possible ionizations (even those known not to occur).[18] Most other modelers[10,17,19–21] have included a few higher polymeric species as well. This study has also included the higher polymers since such an approach is more comprehensive. In addition, a single representative polymer for each connectivity group was selected. With the exception of the linear trimer and the linear tetramer, all the polymers in Table 1 were used.

When dealing with ionized polymers, the exact definition of ionic strength becomes clouded. Throughout this work we assume a calculation of ionic strength based on the charge per silicon atom rather than on the total charge of each polymeric molecule. This is somewhat more realistic since a charge of –1 per silicon atom in the cubic octamer should not contribute to the ionic strength as if it were a single ion of charge –8. It could easily be argued that the charge contribution should count for more than just –1 as well. An additional problem arises if the charge per silicon atom is not an integer. In this case, ionic strength can still be calculated, for example, using a charge of –½. These difficulties arise because the concept of ionic strength was not developed with polymeric ions in mind. In practice, the use of charge per Si atom produces better fits to data, and is therefore justified for that reason.

Data obtained from NMR analysis, pH measurements, and solubility are essential in establishing aqueous silicate species. During the parameter estimation process, numerous combinations of species were used. The resulting set of species is based on the fewest number which could adequately describe the experimental results. Pitzer parameters were determined for interactions of Na^+ with each of the ionic species; Gibbs energies were determined for each silicate species. The resulting parameter values are given in Appendix A.

2.6. Model Predictions

Predictions of speciation in silicate solutions at 25°C are compared with NMR data in Figs. 2–7. In each figure, both axes represent concentrations of the various connectivity groups (mol/kg water); a perfect match between data and calculation would lie on the diagonal line. While there is considerable scatter, the model generally predicts each of the connectivity groups fairly well. Of some concern is the

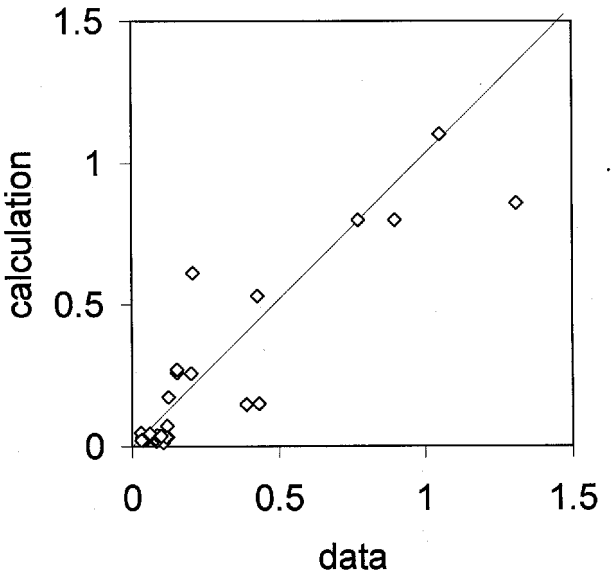

Fig. 2. Monomeric silica (Q^0 connectivity group) at 25°C. Axes represent mol/kg water.

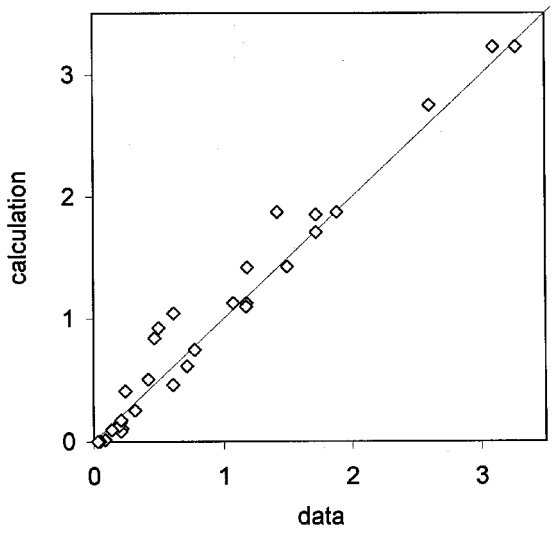

Fig. 3. Dimeric silica (Q^1 connectivity group) at 25°C.

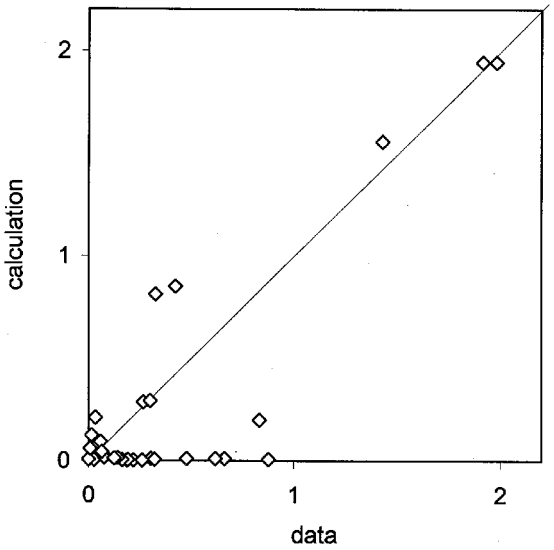

Fig. 4. Cyclic trimer (Q^2_Δ connectivity group) at 25°C.

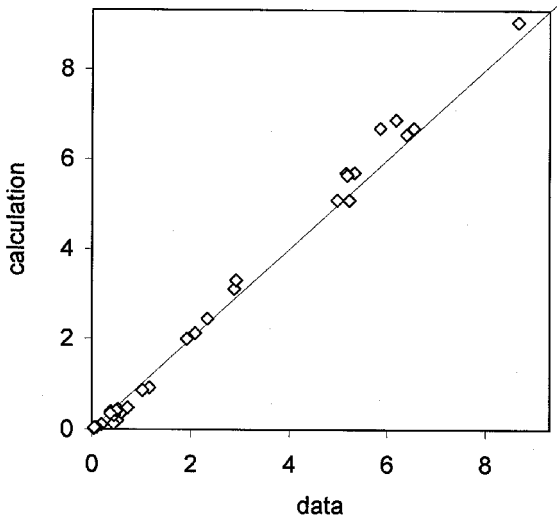

Fig. 5. Cyclic tetramer (Q^2 connectivity group) at 25°C.

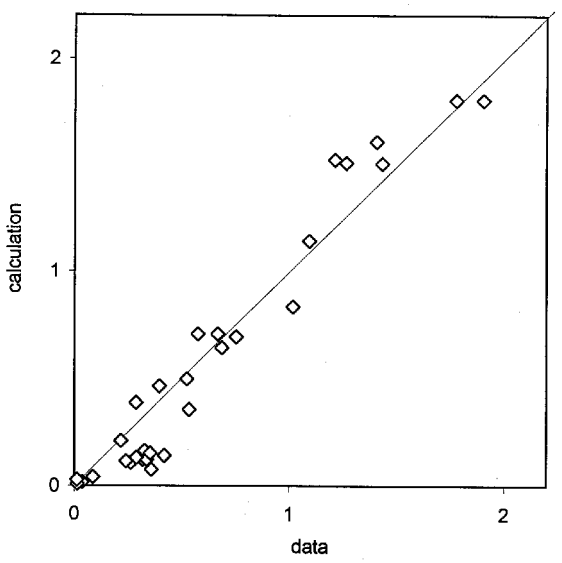

Fig. 6. Prismatic hexamer (Q^3_Δ connectivity group) at 25°C.

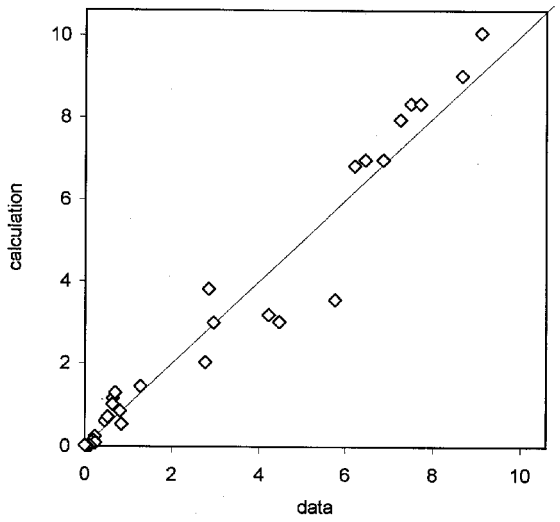

Fig. 7. Prismatic octamer (Q^3 connectivity group) at 25°C.

underprediction of data below 1 *m* for the Q^2_Δ group. However, many of the solutions involved total silica and NaOH concentrations above 10 *m*, the highest being about 20 *m* in each. The model does an excellent job with the more dominant groups Q^2 and Q^3, even to 10 *m* in these species.

Additional model calculations for silicate solutions at 25°C include pH and solubility. In Fig. 8, pH predictions for the same data as the NMR comparisons indicate fairly good agreement through the range from 11.5 to 14. At lower pH values, solubility data from ref. 15 is predicted well by the model, shown in Fig. 9. Finally, silica solubilities in $NaNO_3$ solutions (near neutral pH) are shown in Fig. 10, indicating that the model tracks the data fairly well.

Above 25°C, less data are available, but are still sufficient to construct a reasonable model. NMR data of Kinrade[12] extend to 100°C, and suggest that the distribution of silicate connectivity groups do not change greatly. Figures 11–16 compare model calculations with data, and indicate generally good agreement. Again, underprediction in the Q^2_Δ group is noticeable, although not crucial. Concentrations in these solutions are lower than for those at 25°C. Also, data uncertainty is greater, since the NMR spectra are wider as temperature increases. This creates more overlap between different connectivity groups, making deconvolution more difficult.

Solubility of amorphous silica in water is shown in Fig. 17. Above 100°C, the model tends to slightly overpredict Si in solution, although the excess is not great. No reliable data are available in caustic solutions at high temperatures. However, we intend to conduct some simple solubility tests to obtain such information in the near future, after which some model revision may be justified.

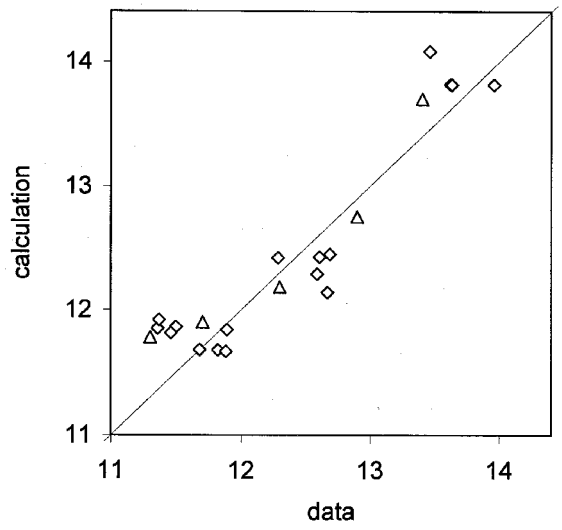

Fig. 8. pH of NMR solutions at 25°C. ◇ Data from ref. 11. Δ Data from ref. 10.

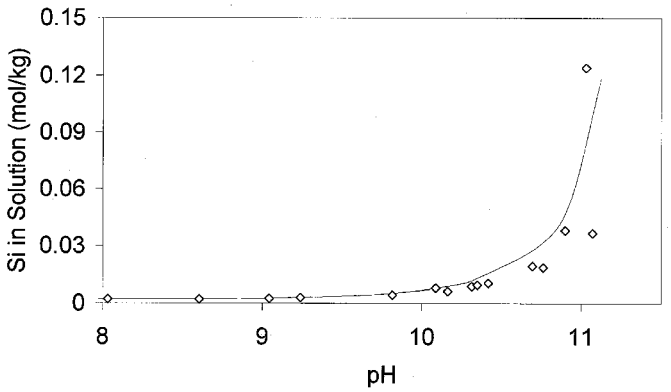

Fig. 9. Solubility of amorphous silica in weakly alkaline solutions at 25°C. ◇ Data from ref. 15. —— Calculations.

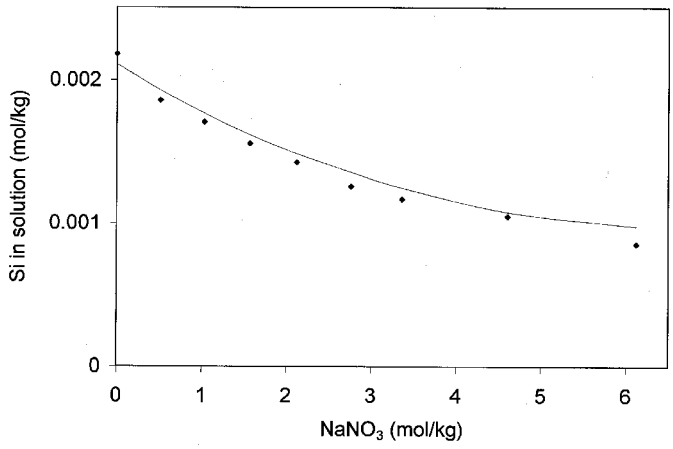

Fig. 10. Solubility of amorphous silica in $NaNO_3$ solutions at 25°C. ◇ Data from ref. 13. —— Calculations.

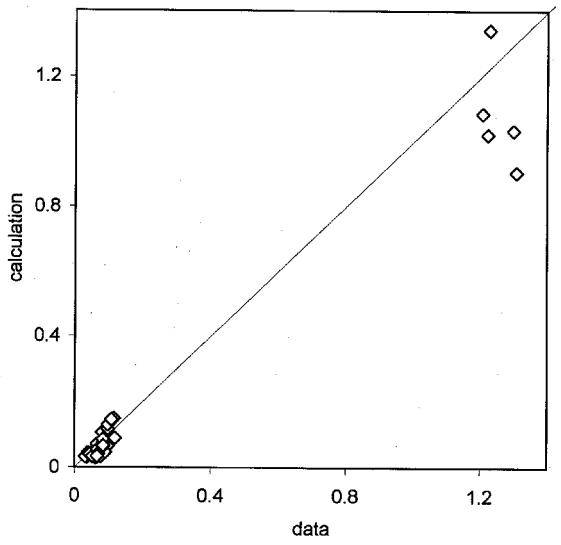

Fig. 11. Silica monomers (Q^0 connectivity group) 30–100°C.

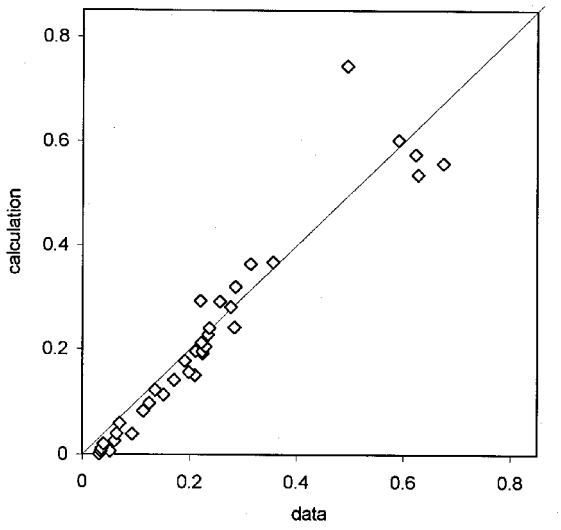

Fig. 12. Silica dimers (Q^1 connectivity group) 30–100°C.

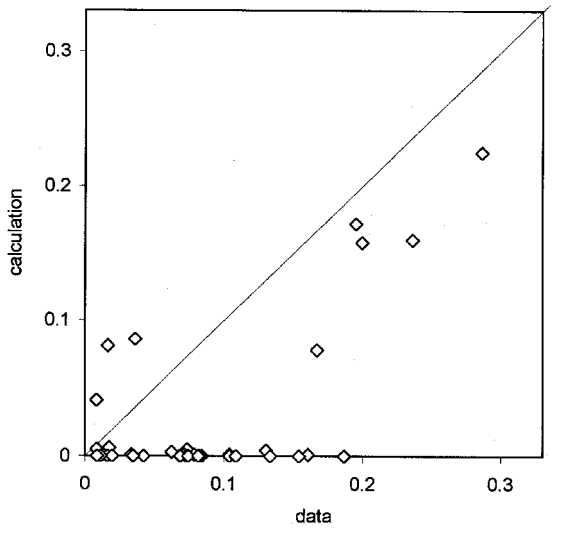

Fig. 13. Cyclic trimer (Q^2_Δ connectivity group) 30–100°C.

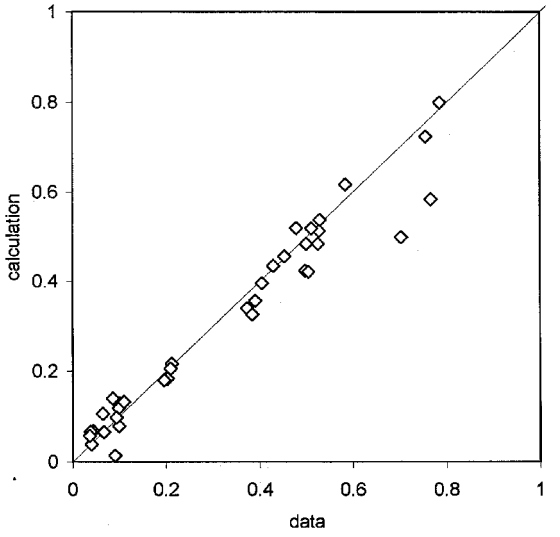

Fig. 14. Cyclic hexamer (Q^2 connectivity group) 30–100°C.

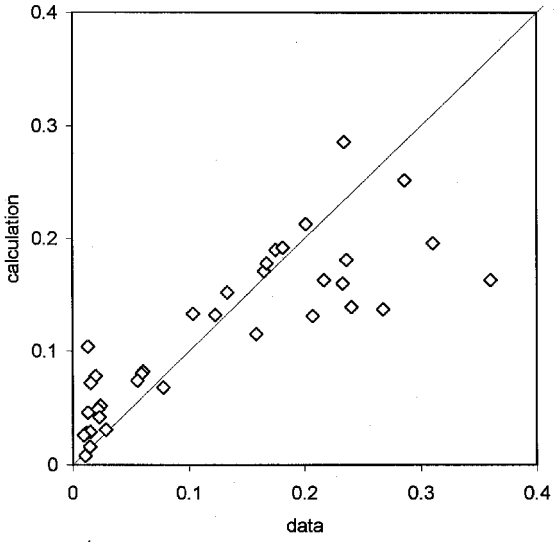

Fig. 15. Prismatic hexamer (Q^3_Δ connectivity group) 30–100°C.

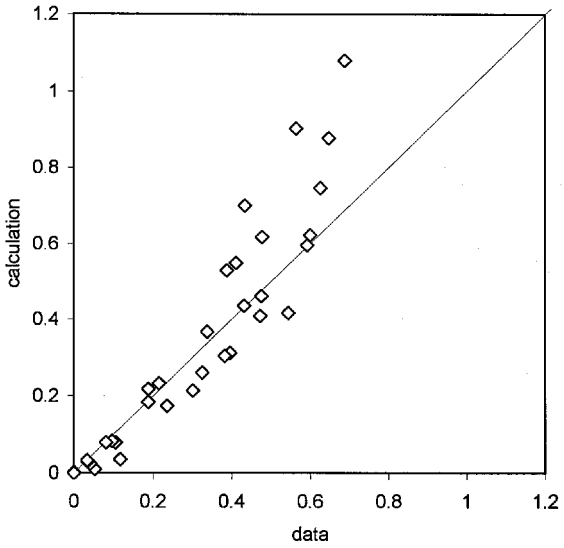

Fig. 16. Prismatic octamer (Q^3 connectivity group) 30–100°C.

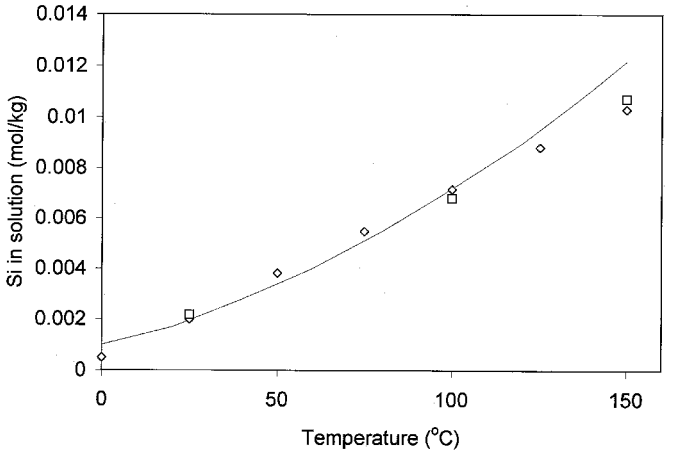

Fig. 17. Solubility of amorphous silica in water.
Data: ◇ Ref. 36, □ Ref. 13. —— Calculations.

2.7. Alumina-Silicate Compounds

Both Al and Si exhibit high solubilities in caustic solutions. However, in solutions containing both elements, solubility drops sharply, due to the formation of aluminosilicate solids. Often these solids contain additional salts, forming zeolites, sodalites, and cancrinites; these all have similar stoichiometries, although they differ in crystal structure and sometimes in solubility. The solids often undergo phase changes after precipitation, generally following the order: amorphous aluminosilicate → zeolite → sodalite → disordered cancrinite → cancrinite. These transitions are temperature dependent — at 25°C they may take months, whereas, at 120°C the appearance of sodalite or cancrinite may occur quickly, either skipping the preliminary stages or else progressing through them very rapidly. Furthermore, at lower temperatures a given crop of solids does not change instantly, so that several phases may be present simultaneously. Solubility behavior may be proportional to each phase present, or may be erratic, since less soluble phases may effectively block access to solution of the more soluble phases.

Many aluminosilicate solids are metastable, i.e., they behave as if in equilibrium long enough to measure their properties. The value of an equilibrium calculation determines where a system wants to go, but does not indicate how long it will take to get there. When metastable states are considered, the result may be a "meta-equilibrium" that does not last indefinitely, but gradually transitions to some other "meta-equilibrium." Thus, meta-stability clouds the concept of true equilibrium, but does introduce a level of practicality that is relevant to aluminosilicate formation especially at lower temperatures.

Thermodynamic data for aluminosilicate formation can be found in many fields, including manufacture of zeolite catalysts, pulp and paper-making, and aluminum refining. For our purposes, the relevance of various data is determined by the similarity of experimental conditions to those expected in SRS tanks or process equipment. For example, commercial zeolites are usually cured at temperatures from 100–200°C, which removes some of the water from the crystal. Solubility of the resulting solid is lowered, and is not characteristic of SRS tank solids, which have always been in contact with a liquid phase. Some industrial data involve actual plant liquors, which may contain small amounts of impurities such as Cl^-, SO_4^{2-}, and CO_3^{2-}. Because SRS tanks also contain small inventories of these ions, such industrial data may be useful, even if the exact solution composition is not known.

Because of the myriad of solid phases (each of which can contain variable amounts of included salt and water), actual modeling requires some level of simplification and subjectivity. Two approaches are outlined below.

Characteristic solids. In this approach, a small number of solids are chosen, but are representative of most situations to be encountered. The characteristic solid in the model may actually represent several solids that actually occur. For example, amorphous aluminosilicate may be the dominant form (and exist almost indefinitely) at 25°C; hydrated zeolite at 60°, and fully crystalline sodalite at 100°C would be the meta-stable solids. The stoichiometries of all three are identical. The characteristic solid would be modeled so as to reflect phase equilibrium with the actual solids at the temperatures where they exist. It is quite useful in predicting solution concentrations although it does not distinguish between the variety of solid phases which may exist.

Multiple solids. Many different solid phases are included in the model database, however, the preferred one must be selected when the calculation is actually performed. Because they are storchiometrically identical, an equilibrium calculation will automatically precipitate the single species with the lowest solubility product. (It is mathematically impossible for an equilibrium code to subjectively select a different metastable phase or a mixture of metastable phases.) The various metastable phases are favored under certain conditions; however, once in the database, it is easy for them to be predicted under very different conditions, where other phases are preferred. Care must be taken to ensure that no phase is calculated outside the temperature and concentration ranges for which its parameters were determined from actual data. For example, the amorphous aluminosilicate can be predicted at low temperatures only by turning off (suppressing) the calculation of zeolite, sodalite, cancrinite and any additional solids. At a higher temperature, a different solid should be selected, since virtually no data exist for amorphous aluminosilicate above about 80°C.

The approach taken in this work is that of characteristic solids for several reasons:

1. The actual solid phases are not always readily identified; solubility data may involve mixed phases, and different researchers may disagree on metastable phases present. Furthermore, included salts and hydration will likely occur in fractional amounts that vary with problem conditions (e.g., temperature, pH, Al or Si concentration).

2. The range of applicability (in temperature, OH^- concentration, and influence of other salts) for individual phases is typically quite small. The subjective selection of a preferred phase for many calculations can be highly uncertain.

3. The greatest variability (and uncertainty) occurs in systems without neutral salts such as $NaNO_3$ (i.e., $NaOH—SiO_2—Al(OH)_3$). Most research above 50°C suggests that even small amounts of $NaNO_3$ yield a nitrated aluminosilicate, and that the solids tend to be the higher crystalline forms sodalite and cancrinite.

Barrer and coworkers[22–23] have evaluated many different salt solutions and identified the preferred solid forms. Two solids that have particular relevance to this work are hydroxy-sodalite and nitrate-cancrinite.

Hydroxy-sodalite. In highly caustic solutions, some NaOH is taken up into the crystal structure, along with water of hydration. While the amounts of each may vary, a standard formulation is

$$\left(\mathrm{Na\ Al\ Si\ O_4}\right)_6\left(\mathrm{NaOH}\right)_2\left(\mathrm{H_2O}\right)_2\ , \tag{6}$$

which is the form assumed in this model. Solubility data vary because of difficulty in achieving true equilibrium (especially at lower temperatures), measurement error, presence of impurities in both solution and solid, and effects of precipitation kinetics on crystal structure. Thus, the task of modeling is to provide a credible description of many diverse data.

Data used for this system are listed in Table 3. The Gibbs Energy of Formation for the solid was obtained by regressing most of the data from the table. Model recalculations of solubility are compared with some of the data in Figs. 18–23. In Figs. 18–20, the model generally tracks the Al data of Ejaz[24] at lower temperatures, although it is noticeably lower than the Si measurement. The solid measured by these researchers was somewhat rich in Si, as compared to Eq. (6), where Al/Si ratio is 1. Also, the trend reversals in Ejaz data (Figs. 19, 20, 21) are likely measurement errors, and illustrate both the uncertainty in data and the difficulty of consistent measurement in metastable systems. Figure 21 shows this same effect at 80°C, although data by Barrer[22] are also included. The calculation matches the trend in the Ejaz data, and is generally consistent with both sets of data. Both sets of data assume metastable equilibrium, although the solid phases are possibly different. The model is certainly as consistent with the data as the two data sets are with each other.

Table 3. Solubility data for hydroxy-sodalite

Reference	T (°C)	NaOH	Remarks
24	30–80	3–4.4 *m*	probably amorphous aluminosilicate
22	80	1–6 *M*	sodalite
25	90	>4 *M*	Al in excess, solid unknown
26	50–150	3.2 *M*	Actual spent Bayer liquor, solid unknown
27	95	1–3 *M*	Simulated Bayer liquor, solid is sodalite

Solubility at higher temperatures is illustrated in Figs. 22–23. Both sets of data describe spent Bayer liquor, so they include small amounts of other ions such as CO_3^{2-}, Cl^-, and SO_4^{2-}. In Fig. 22, the model exaggerates the negative slope of the data below 90°C, and underpredicts most of the solubility points above 90°C. However, the uncertainty in the data is illustrated by the single point at 127°C (from a different experimental run) which is lower than the model. In addition, data at 95°C from a different researcher also lies below the model calculation, as shown in Fig. 23. Thus, the model does a credible job of reflecting most of the data, although close quantitative agreement is elusive due to the scatter and diversity of the data.

Nitrate-cancrinite. In solutions containing $NaNO_3$, this salt is taken into the crystal structure along with water of hydration. In solutions containing both NaOH and $NaNO_3$, the nitrate appears to dominate. The preferred stoichiometry involves fractional amounts,[23,28] and the form adopted here is:

$$(\mathrm{Na\ Al\ SiO_4})_6\ (\mathrm{NaNO_3})_{1.68}\ (\mathrm{H_2O})_{4.1}$$

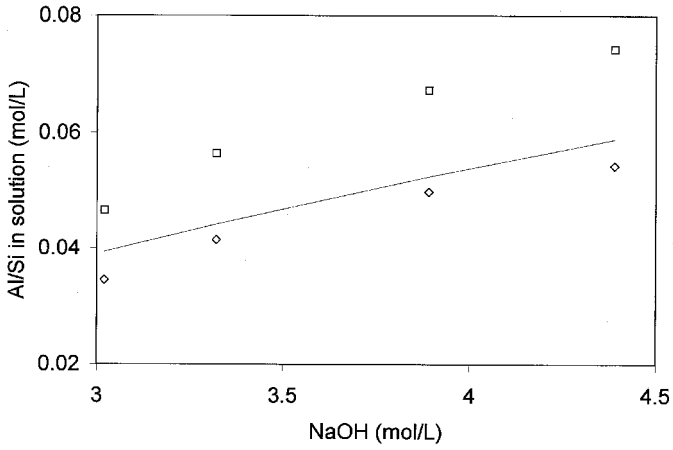

Fig. 18. Solubility of hydroxy-sodalite at 30 °C. Data of ref. 24 for □ Si, ◇ Al. —— Calculations.

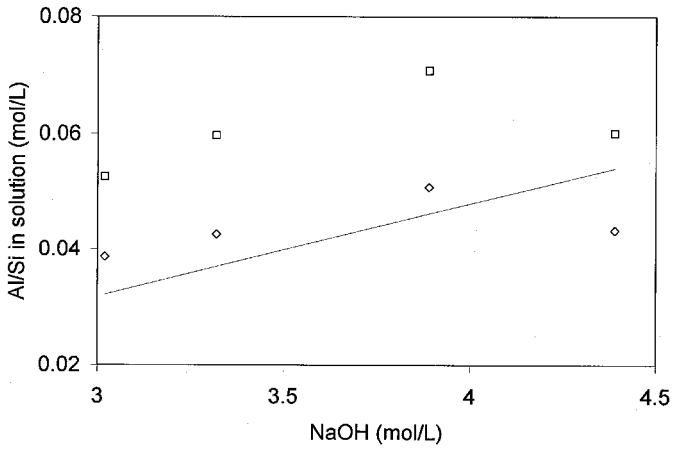

Fig. 19. Solubility of hydroxy-sodalite at 50 °C. Data of ref. 24 for □ Si, ◇ Al. —— Calculations.

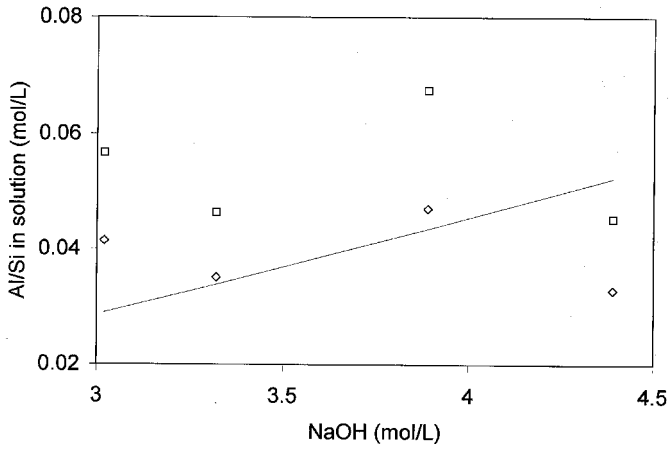

Fig. 20. Solubility of hydroxy-sodalite at 65 °C. Data from ref. 24: □ Si, ◇ Al. —— Calculations.

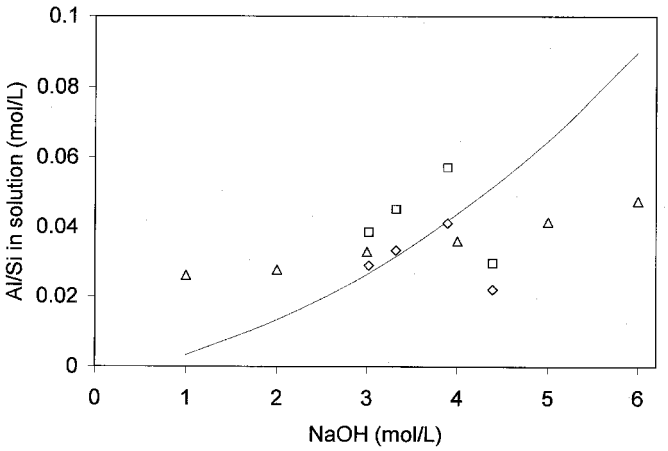

Fig. 21. Solubility of hydroxy-sodalite at 80 °C. Data: Δ Ref. 22, □ Ref. 24 (Si), ◇ Ref. 24 (Al). —— Calculations.

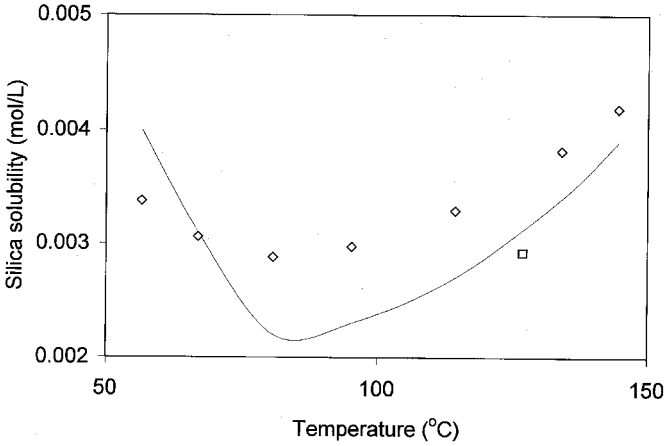

Fig. 22. Solubility of hydroxy-sodalite in spent Bayer liquor (3.2 *M* NaOH, minor constituents unknown). ◇ □ Data from ref. 26. —— Calculations.

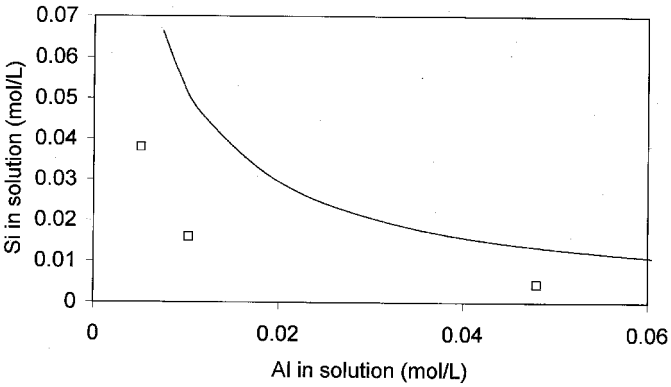

Fig. 23. Solubility of hydroxy-sodalite at 95°C in simulated Bayer liquor (2.5 *M* NaOH, 0.3 *M* Na_2CO_3, 0.1 *M* NaCl, 0.1 *M* Na_2SO_4). □ Data from ref. 27. —— Calculations.

Data for this solid are sparse, and somewhat qualititative; hence, there is greater uncertainty in modeling its solubility behavior. Briefly, at 80°C, Barrer et al.[22] noted formation in 4 *M* NaOH as $NaNO_3$ concentration was decreased from 2 *M* to 0.002 *M*. Their observations are shown in Table 4, where they are compared to model calculations. Kinetic data at both 95°C and 110°C[29] indicate that if either Al or Si is present in large excess, the other will exhibit solubility of about 0.001 *M* (presumably in equilibrium with nitrate-cancrinite). Finally, Beahm has estimated Gibbs energy at 25°C by combining a heuristic value for entropy with a measured value for enthalpy.[28] This evaluation is described in Appendix B, and is used with caution, since it has a high uncertainty. However, no other data are available below 80°C. Using these qualitative data, the Gibbs Energy for the solid has been estimated in the range 25–110°C, and will be used in verification calculations in the next section.

Table 4. Nitrate-cancrinite solubility at 80°C in 4 mol/kg NaOH

$NaNO_3$ (mol/kg)	Solid phase from ref. 22	Solid phase calculated result
2.0	Cancrinite	Cancrinite
0.99	Cancrinite + trace sodalite	Cancrinite
0.066	Cancrinite + trace sodalite	Cancrinite
0.018	Cancrinite + trace sodalite	Cancrinite (98%) + sodalite
0.013	Cancrinite + sodalite	Cancrinite (67%) + sodalite
0.007	Cancrinite + sodalite	Cancrinite (31%) + sodalite
0.0039	Cancrinite + sodalite	Cancrinite (12%) + sodalite
0.0023	sodalite	Cancrinite (2%) + sodalite

3. VERIFICATION AND DISCUSSION

The parameters in Appendix A define the model for calculation of phase equilibria in electrolyte solutions. Validation is accomplished by the ability of the model to match experimental data. At a minimum, the model should match the data used to regress model parameters. This has generally been the case, as has been demonstrated in the previous section. In addition, it should match other data on different systems, which have not been used directly to obtain model parameters.

An ideal opportunity for the latter type of analysis involves SRS simulant solutions.[30] These have been formulated to represent tank wastes commonly encountered at Savannah River. There are three different solutions, termed "Average," "High-OH," and "High-NO_3," whose compositions can be obtained from ref. 30. As described below, several kinetic studies have indicated that standard SRS waste simulants may precipitate solids under various conditions.

When seeded with gibbsite at room temperature, both the Average and High-NO_3 solutions showed noticeable decreases in soluble aluminum, whereas the High-OH simulant indicated a slight increase.[31] This is consistent with model calculations, which predict gibbsite precipitation at 25°C for the Average and High-NO_3 simulants. This behavior is depicted in Fig. 24, where the symbols indicate transient measurements and solid horizontal lines represent equilibrium amounts. The model did not predict such precipitation for the High-OH case, whose rise in soluble Al could be explained by simple dissolution of the seed particles.

The High-NO_3 simulant was investigated in experiments at Sandia National Laboratory (SNL).[32] The solution was made up at room temperature and its solubility evaluated at six different temperatures. Duplicate silicon measurements were taken and generally agree well with each other. The experimental solubilities are compared with calculated values in Fig. 25. Aluminosilicate was predicted to form above 30°C by the model (sodalite at 40°C, cancrinite at higher temperatures). Also, gibbsite was predicted to form up to 50°C. The agreement is quite good above 50°C, although not as close below this temperature. The SNL researchers noted that the experimental system may not have been at equilibrium below 40°C.

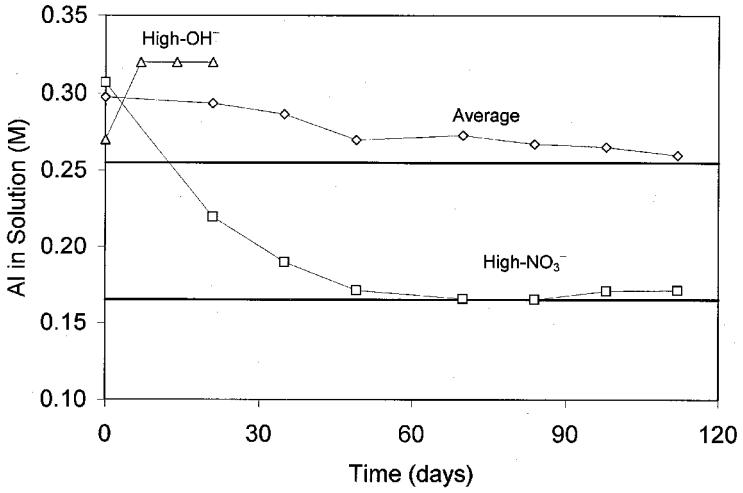

Fig. 24. Precipitation in SRS simulated solutions at 25 °C (seeded with gibbsite). Data from ref. 31. Horizontal lines are equilibrium calculations.

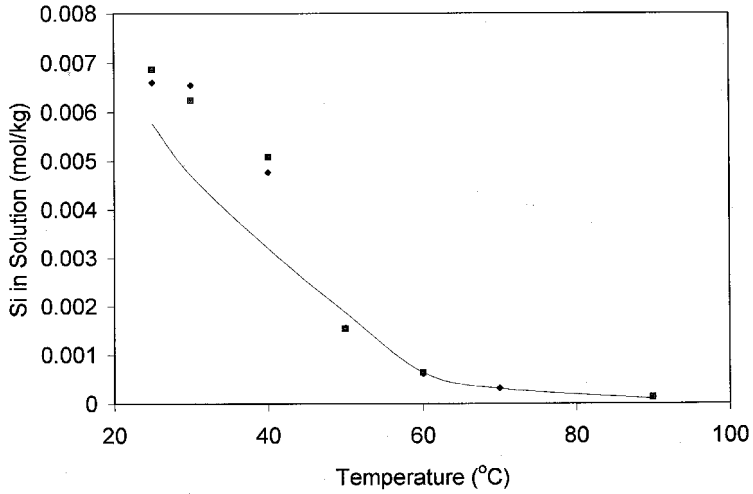

Fig. 25. Precipitation in SRS High-NO_3 simulant. ■ ♦ Data from ref. 32. — Model prediction.

Solutions of SRS Average simulant were evaluated at 55° and 80°C in studies at PNNL.[33] Over time, the concentration approaches steady state values as shown in Fig. 26. Model calculations are also shown in the figure (horizontal lines), and indicate good agreement at 80°C, suggesting consistency with data of Barrer et al.[22] At 55°C, the model prediction is somewhat higher than the data, and indicates underprediction of NO_3-cancrinite formation. These data are in some disagreement with those of Fig. 25, where the model appears to closely match solubility data in this temperature range.

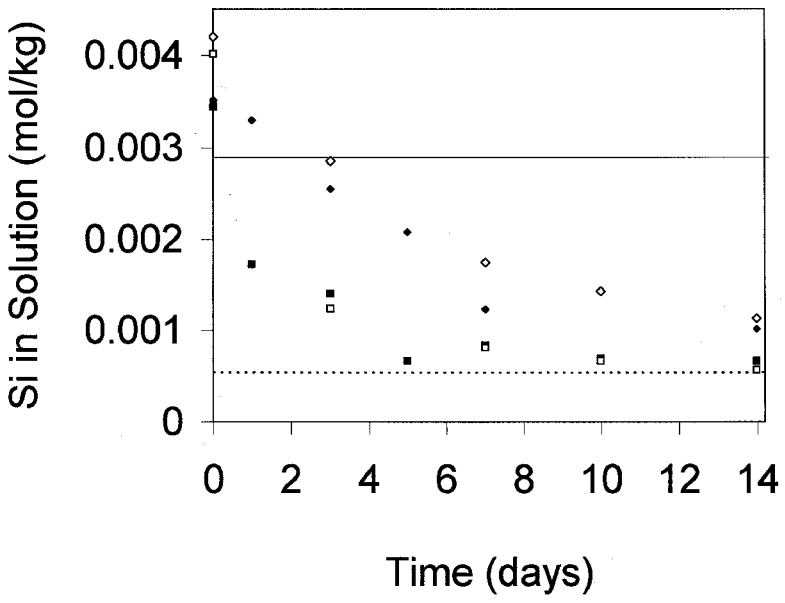

Fig. 26. Precipitation in SRS average simulant. Data from ref. 32: ◊ ♦ 55°C, □ ■ 80°C. Calculation: — 55°C, --- 80°C.

4. SATURATION IN SRS TANKS

The model (i.e., code plus input parameters), described in the previous sections, has been applied to a number of existing SRS tanks to determine the state of saturation in the tanks. If supersaturated, then additional precipitation may take place. This is of general concern for a variety of reasons, but of paramount concern is the fouling that could occur during Cs-removal operations.

Information on tank waste inventories was gleaned from an extensive database of sample measurements by Jeff Pike, and forwarded to ORNL personnel via e-mail.[34] It was important that tanks under consideration needed recent (i.e., within the last year) measurement records. Indeed, for most of these tanks, measurements are made every few months, so numerous recent data are available; this analysis included only the most recent. It is also noteworthy that these recent measurements include samples for Si concentration. The inventories of major components were converted to molal concentrations, and are shown in Table 5. Using the inventories in Table 5, phase equilibrium calculations were performed at 25°C, 40°C, and 60°C, producing the results shown in Table 6. These temperatures are important, since Cs removal is expected to occur at 25°C, although most tanks exist at 35–40°C due to radioactive heating. The higher temperature (60°C) is considered since unknown processes may at some time allow additional temperature increase.

Tank 46 is the evaporator drop tank, and considerable precipitation occurs as expected. Several of the other tanks do exhibit slight supersaturation at 25°C, with gibbsite the most common precipitate. At higher temperatures gibbsite dissolves, but aluminosilicates begins to form. Because the tanks are maintained at temperatures of 35°–40°C, it is likely they are in equilibrium with gibbsite. It is also possible that they are in equilibrium with sodalite and/or cancrinite as well, and the small amount of solids calculated at 40° and 60°C is simply an error in the calculation. However, it is likely that cancrinite solubility decreases as temperature increases (cf. Figs. 25 and 26), and the calculations are correct. Hence, either the tanks are slightly oversaturated or the analytical measurements are slightly in error.

It is also interesting to note the formation of oxalate solids in a few of the tanks, indicating that these species are likely near saturation. Oxalate solubility changes very little with temperature, but decreases rapidly as ionic strength increases[9] and as pH decreases. Thus, as temperature increases, ionic strength increases in Tank 46 due to dissolution of solids. Also, pH in all tanks decreases as temperature increases, due to the

changing water dissociation coefficient. For oxalate inventory at or above saturation, these effects result in increasing precipitation as temperature increases.

Table 5. SRS tank measurement data

Tank	Sample Date	Specific Gravity	pH	Concentrations (mol/kg) K^+	Si	Na^+
46	12/05/00	1.4290	14.65	0.1217	0.0051	18.8285
43	12/23/00	1.2110	14.55	0.0143	0.0042	5.4725
40	07/10/00	1.1400	14.00	0.0004	0.0014	2.1578
38	02/26/00	1.0492	13.98	0.0270	0.0027	1.4858
33	12/02/98	1.4400	>14.00	0.0029	0.0002	2.3261
32	02/15/01	1.4470	14.55	0.0561	0.0024	10.0957
30	02/15/01	1.2900	14.38	0.0254	0.0017	5.3734
29	02/15/01	1.1000	14.20	0.0289	0.0017	2.2588
26	02/27/01	1.3513	14.73	0.0583	0.0021	9.7078
24	02/04/01	1.0352	14.06	0.0013	0.0013	0.8804
23	02/04/01	1.0196	13.49	0.0013	0.0033	0.4695
22	02/04/01	1.0350	13.98	0.0013	0.0013	0.7959
21	02/04/01	1.0363	14.01	0.0013	0.0014	0.8147

Tank	Anion Concentrations (mol/kg) $AlOH_4^-$	$C_2O_4^{2-}$	Cl^-	CO_3^{2-}	F^-	NO_2^-	NO_3^-	OH^-	PO_4^{3-}	SO_4^{2-}
46	0.7191	0.0077	0.0477	0.0138	0.0073	2.2277	2.0438	13.7728	0.0192	0.0155
43	0.2974	0.0063	0.0061	0.0551	0.0058	0.9143	1.3605	2.7210	0.0058	0.0207
40	0.0000	0.0238	0.0099	0.0099	0.0148	0.2772	0.6237	0.9900	0.0208	0.0564
38	0.0523	0.0060	0.0029	0.0628	0.0055	0.2860	0.4781	0.5230	0.0055	0.0054
33	0.0281	0.0003	0.0013	0.0684	0.0008	0.0288	0.6909	1.3520	0.0002	0.0446
32	0.8533	0.0065	0.0124	0.0337	0.0061	2.0546	1.9760	5.1197	0.0082	0.0125
30	0.3349	0.0057	0.0066	0.1256	0.0074	0.9271	1.6638	2.1243	0.0052	0.0283
29	0.1033	0.0064	0.0035	0.1342	0.0059	0.4015	0.4365	1.0325	0.0038	0.0059
26	0.3547	0.0072	0.0169	0.0343	0.0062	1.2475	1.9215	6.0407	0.0089	0.0344
24	0.0101	0.0006	0.0001	0.0101	0.0005	0.2395	0.0616	0.5457	0.0005	0.0005
23	0.0101	0.0006	0.0006	0.0504	0.0005	0.1835	0.0393	0.1311	0.0005	0.0010
22	0.0101	0.0006	0.0006	0.0503	0.0005	0.1528	0.0462	0.4826	0.0005	0.0005
21	0.0101	0.0006	0.0006	0.0101	0.0007	0.1921	0.0654	0.5230	0.0006	0.0005

Table 6. Phase equilibrium results for SRS tanks

	Precipitation at 25°C		Precipitation at 40°C		Precipitation at 60°C	
Tank	Solid species	Amount[a]	Solid species	Amount[a]	Solid species	Amount[a]
46	Na_2SO_4, Na_2SO_4·NaF	98	Na_2SO_4, Na_2SO_4·NaF	85	Na_2SO_4·NaF	36
	$NaNO_3$	92	$NaNO_3$	75	$NaNO_3$	18
	$NaNO_2$	97	$NaNO_2$	92	$NaNO_2$	72
	$Na_2CO_3·H_2O$	78	$Na_2CO·H_2O$	69	$Na_2CO_3·H_2O$	64
					$Na_2C_2O_4$	98
43	$Al(OH)_3$	3				
40						
38	$Al(OH)_3$, sodalite	22	sodalite	3	cancrinite	3
33						
32	$Na_2C_2O_4$	1	$Na_2C_2O_4$	29	$Na_2C_2O_4$	57
30	$Al(OH)_3$	33				
29	$Al(OH)_3$	19	sodalite	4	cancrinite	<1
26			$Na_2C_2O_4$	<1	$Na_2C_2O_4$	25
24			sodalite	5	cancrinite	7
23	cancrinite	14	sodalite	24	cancrinite	24
22			sodalite	7	cancrinite	8
21			sodalite	6	cancrinite	9

[a] Percentage (mol) of principal anion in solid(s). For sodalite or cancrinite, percent of Al precipitated.

5. DILUTION STRATEGIES

The Salt Waste Processing Facility (SWPF) is planning to handle wastes that may be at or above saturation, especially with respect to aluminosilicates. Estimated feed streams for 13 years of operation were recently forwarded to ORNL by Jeff Pike of SRS,[35] and are shown in Appendix C. We seek to evaluate each feed solution for precipitation, and determine an optimal dilution strategy to reduce the total sodium ion concentration to 5.6 *M*.

To begin, we consider only the dominant species, ignoring NH_4NO_3, $Na_2U_2O_7$, $Sr(OH)_2$, HgO, and sludge. (These constitute less than 0.1% of the solution inventories.) The component listed as "other salt" was assumed to be NaCl. The weight fractions were then converted to molality units and a series of calculations performed for each year separately. As shown in Table 7, calculation of phase equilibrium for each feed solution indicated that gibbsite would precipitate at 25°C each year except year 8. Thus, to prevent any precipitation, it was necessary to use caustic dilutions for each year except year 8, where a water dilution proved to be adequate. For year 13, initial sodium ion concentration is lower than 5.6 *M*; hence, a tiny addition of concentrated caustic was sufficient to dissolve all solids, without raising the Na^+ concentration appreciably.

The feed solutions do not mention any silica inventory. Hence, the model was used to calculate silica needed to precipitate a solid phase containing silica (in every case it was the sodalite). These values are given in Table 7, column 3. Most estimates of silica content in SWPF feed are below these values; hence, precipitation of aluminosilicates is not likely.

For all feed compositions, except years 8 and 13, it was necessary to calculate an optimal caustic dilution. The optimal dilution was that which minimized the addition of sodium, while preventing solids formation and lowering the overall sodium concentration to 5.6 *M*. This was accomplished by using the weakest caustic concentration which yielded no solid precipitate and resulted in 5.6 *M* sodium. (A caustic concentration higher than the optimal value would dissolve all solids, but more would be required; a caustic concentration lower than the optimal one would not dissolve all solids unless extremely large quantities were used.).

For each feed solution, various concentrations of caustic were examined and the optimum determined. These values are listed in Table 7. In column 4 is given the caustic concentration of the optimal dilution, and

in columns 5 and 6 the amount to be added (liters of caustic solution per kg feed solution, and liters of caustic per liter of feed solution).

Table 7. SWPF feed stream dilution and precipitation evaluation at 25 °C

year	precipitation[a]	Si[b] (m)	Dilution caustic		
			NaOH (*M*)	ratio[c] (L/kg)	ratio[d] (L/L)
1	gibbsite	0.0065	2.9	0.283	0.366
2	gibbsite	0.0076	2.7	0.274	0.352
3	gibbsite	0.0068	3.6	0.362	0.473
4	gibbsite	0.0067	3.8	0.346	0.449
5	gibbsite	0.0080	2.3	0.234	0.297
6	gibbsite	0.0072	2.4	0.229	0.292
7	gibbsite	0.0063	3.3	0.319	0.414
8	none	0.0088	0	0.139	0.176
9	gibbsite	0.0065	2.9	0.284	0.369
10	gibbsite	0.0047	3.9	0.163	0.205
11	gibbsite	0.0078	4.3	0.162	0.204
12	gibbsite	0.0074	4.4	0.216	0.273
13	gibbsite	0.0060	10	0.05	0.059
			3	0.24	0.283
avg	gibbsite	0.0064	5.6 *M*		0.15
High-NO_3	gibbsite	0.0042	5.6 *M*		0.31
High-OH	—	0.0115			

[a] Initial feed stream precipitation.

[b] Silica solubility. Above this amount results in aluminosilicate precipitation.

[c] Amount of diluting caustic (L) required per kg of feed. No dilution required for High-OH simulant (no precip., already 5.6 *M* Na^+).

[d] Amount of diluting caustic (L) per L of feed solution.

Using year 1 as an example, if 0.283 L of 2.9 *M* NaOH are added to each kg of feed (0.366 L of 2.9 *M* NaOH per L of feed) then no precipitation will occur. However, if 2.8 *M* NaOH is used, then precipitation will still occur (unless the dilution is extremely high). If 3.0 *M* NaOH is used, then a higher amount of diluting caustic must be added to achieve 5.6 *M* Na^+.

It is important to note that the overall Na^+ concentration used in this analysis differed slightly from the values given in Appendix C (third line from the bottom of Table C.1). For the calculation, it was necessary to maintain a charge balance; hence, the initial Na^+ concentration reflected only components in the first 9 rows of Table C.1. Thus, the values in Table 7 may be in error by about 2% (relative to the total Na^+ values in Table C.1).

It is important to note the use of different units and measures. Feed solution data were supplied in weight percent. These are easily converted to make mole inventories (per kg feed solution), which form the input to the model. Dilution strategies at SRS call for caustic additions and final solution units of molarity. Conversion from mole inventories (or molalities) to molarity was done using the feed density supplied by SRS (see Appendix B). Finally, the conversion of caustic solution concentrations (molarity) to mole inventories was done using the data for NaOH solutions from the CRC handbook.[36]

Also shown in Table 7 (last 3 lines) are analyses done for SRS simulant solutions.[30] All three simulants contain 5.6 M Na^+, so dilutions were simulated using 5.6 *M* NaOH. Because no solids form in the High-OH simulant, no dilution was necessary.

6. CONCLUSIONS

The ORNL model has been used to predict precipitation of Al and Si solids in SRS tanks and SWPF waste streams. The model itself was validated on solubility data of Al solutions, Si solutions, and combined Al-Si solutions. It is consistent with experiments at SRS, SNL and PNNL using SRS simulant solutions at temperatures between 25 and 80°C.

The model predicts that most of the SRS tanks are slightly oversaturated at 25°C with respect to gibbsite. As temperatures rise above 25°C, most remain slightly supersaturated, but the preferred solid is an aluminosilicate. A few of the tanks also indicate supersaturation with respect to oxalate solids.

Gibbsite precipitation was also predicted to occur in most of the SWPF feed streams. With sufficient silicate present, the preferred solid becomes sodalite at 25°C; however, the threshold Si required is generally higher than the expected Si inventories. All years except year 13 required some dilution to lower the sodium ion concentration to 5.6 *M*. Year 8 required only a water dilution. All other years require a caustic dilution (to prevent solids formation) using 2–5 *M* NaOH solution in amounts of about 0.2–0.3 L/kg feed solution. Thus, it appears that minimal dilutions will be required to meet SWPF requirements.

7. REFERENCES

1. C. F. Weber and E. C. Beahm, *Chemical Modeling of Waste Sludges*, ORNL/TM-13200, Lockheed Martin Energy Research Corp., Oak Ridge National Laboratory (1996).
2. R. D. Hunt et al., *Waste Preparation and Transport Chemistry: Results of the FY2000 Studies*, ORNL/TM-2000/298, UT Battelle, LLC, Oak Ridge National Laboratory (2000).
3. G. Eriksson, "Thermodynamic Studies of High Temperature Equilibria. XII. SOLGASMIX, A Computer Program for Calculation of Equilibrium Compositions in Multiphase Systems," *Chemica Scripta* **8**, 100 (1975).
4. C. F. Weber, "Convergence of the Equilibrium Code SOLGASMIX," *J. Comp. Phys.* **145**, 655 (1998).
5. K. S. Pitzer, "Thermodynamics of Electrolytes. I. Theoretical Basis and General Equations," *J. Phys. Chem.* **77**, 268 (1973).
6. K. S. Pitzer, "Ion Interaction Approach: Theory and Data Correlation," in K. S. Pitzer, ed., *Activity Coefficients in Electrolyte Solutions*, 2nd Ed., CRC Press, Boca Raton, Florida (1991).
7. D. J. Wesolowski, "Aluminum Speciation and Equilibria in Aqueous Solution: I. The Solubility of Gibbsite in the System Na-K-Cl-OH-$Al(OH)_4$ from 0 to 100°C," *Geochim. Cosmochim. Acta* **56**, 1065 (1992).
8. A. S. Russell, J. D. Edwards, and C. S. Taylor, "Solubility and Density of Hydrated Aluminas in NaOH Solutions," *J. Metals* **7**, 1123 (1955).
9. C. F. Weber, *Thermodynamic Modeling of Savannah River Waste Solutions*, Draft letter report (April 4, 2001).
10. I. L. Svensson, S. Sjöberg, and L.-O. Öhman, "Polysilicate Equilibria in Concentrated Sodium Silicate Solutions," *J. Chem. Soc. Far. Trans. 1* **82**, 3635 (1986).
11. A. V. McCormick, A. T. Bell, and C. J. Radke, "Quantitative Demonstration of Siliceous Species in Sodium Silicate Solutions by Silicon-29 NMR Spectroscopy," *ZEOLITES* **7**, 183 (1987).
12. S. D. Kinrade and T. W. Swaddle, "Silicon-29 NMR Studies of Aqueous Silicate Solutions. 1. Chemical Shifts and Equilibria," *Inorg. Chem.* **27**, 4253 (1988).
13. W. L. Marshall, "Amorphous Silica Solubilities — I. Behavior in Aqueous Sodium Nitrate Solutions; 25–300°C, 0–6 Molal," *Geochim. Cosmochim. Acta* **44**, 907 (1980).
14. W. L. Marshall and J. M. Warakomski, "Amorphous Silica Solubilities — II. Effect of Aqueous Salt Solutions at 25°C," *Geochim. Cosmochim. Acta* **44**, 915 (1980).

15. G. B. Alexander, W. M. Heston, and R. K. Iler, "The Solubility of Amorphous Silica in Water," *J. Phys. Chem.* **58**, 453 (1954).

16. D. P. Zarubin and N. V. Nemkina, "The Solubility of Amorphous Silica in an Alkaline Aqueous Media at a Constant Ionic Strength," *Russ. J. Inorg. Chem.* **35**(1), 16 (1990).

17. J. Eikenberg, *On the Problem of Silica Solubility at High pH*, PSI-Bericht Nr. 74, Paul Scherrer Institut (1990).

18. J. SefčíK and A. V. McCormick, "Thermochemistry of Aqueous Silicate Solution Precursors to Ceramics,"*AIChE Journal* **43**(11A), 2773 (1997).

19. P. Caullet and J. L. Guth, "Observed and Calculated Silicate and Aluminosilicate Oligomer Concentrations in Alkaline Aqueous Solutions," in M. L. Occelli and H. Robson, eds., *Zeolite Synthesis*, American Chemical Society, Washington, D.C. (1989).

20. I. Grenthe, J. Fuger, R. J. M. Konings, R. M. Lemire, A. B. Muller, C. Nguyen-Trung, and H. Wanner, *Chemical Thermodynamics of Uranium*, North-Holland, Amsterdam, Netherlands (1992).

21. S. Sjöberg, L.-O. Öhman, and N. Ingri, "Equilibrium and Structural Studies of Silicon (IV) and Aluminium (III) in Aqueous Solution. 11. Polysilicate Formation in Alkaline Aqueous Solution, A Combined Potentiometric and ^{29}Si NMR Study," *Acta Chem. Scand. A* **39**, 93 (1985).

22. R. M. Barrer, J. F. Cole, and H. Sticher, "Chemistry of Soil Minerals. Part V. Low Temperature Hydrothermal Transformations of Kaolinite," *J. Chem. Soc.* (*A*), 2475 (1968).

23. R. M. Barrer, J. F. Cole, and H. Villiger, "Chemistry of Soil Minerals. Part VII. Synthesis, Properties, and Crystal Structures of Salt-filled Cancrinites," *J. Chem. Soc.* (*A*), 1523 (1970).

24. T. Ejaz and A. G. Jones, "Solubility of Zeolite A and Its Amorphous Precursor under Synthesis Conditions," *J. Chem. Eng. Data* **44**, 574 (1999).

25. L. P. Ni, G. L. Perekhrest, and T. V. Solenko, "The Solubility of Sodium Aluminosilicate in Aluminate Solutions," *J. Appl. Chem. USSR* **37**(1), 31 (1964).

26. M. Jamialahmadi and H. Müller-Steinhagen, "Determining Silica Solubility in Bayer Process Liquor," *J. Materials* **50**(11), Suppl. S, 44 (1998).

27. H. Park and P. Englezos, "Thermodynamic Modeling of Sodium Aluminosilicate Formation in Aqueous Alkaline Solutions," *Ind. Eng. Chem. Res.* **38**(12), 4959 (1999).

28. K. O. Bennington and R. R. Brown, *The Enthalpy of Formation of Synthetic Cancrinite*, Rept. 8778, Bureau of Mines (U.S. Dept. of Interior) (1983).

29. W. R. Wilmarth, D. D. Walker, S. D. Fink, *Sodium Aluminosilicate Formation in Tank 43H Simulants*, WSRC-TR-97-00389, Rev. 0, Westinghouse Savannah River Company (1997).
30. D. D. Walker, *Preparation of Simulant Waste Solutions*, WSRC-TR-99-00116 (1999).
31. D. D. Walker, personal communication via e-mail (March 2001).
32. J. L. Krumhansl, e-mail to C. F. Weber (April 23, 2001).
33. Y. Su, L. Li, J. S. Young, and M. L. Balmer, *Investigation of Chemical and Thermal Stabilities of Cs-Loaded UOP IONSIV® IE-911 Ion Exchange (Final Report)*, PNNL-13392-2, Pacific Northwest National Laboratory (March, 2001).
34. Jeff Pike, e-mail to C. F. Weber (March 28, 2001).
35. Jeff Pike, memo to J. T. Carter, HLW-SDT-2001-00071, February 21, 2001.
36. *CRC Handbook of Chemistry and Physics*, 59th Ed. (1978).
37. W. F. Linke, *Solubilities*, 4th ed., Vol. II, D. Van Nostrand Co., Princeton, New Jersey (1958).
38. HSC Chemistry for Windows, Version 2.0, Outokumpu Research, May 31, 1994.
39. C. F. Weber, E. C. Beahm, and J. S. Watson, "Modeling Thermodynamics and Phase Equilibria for Aqueous Solutions of Trisodium Phosphate," *J. Soln. Chem*. **28**(11), 1207 (1999).
40. S. He and J. W. Morse, "The Carbonic Acid System and Calcite Solubility in Aqueous Na-K-Ca-Mg-Cl-SO_4 solutions from 0 to 90°C," *Geochim. Cosmochim. Acta* 57, 3533–54 (1993).
41. C. F. Weber, E. C. Beahm, D. D. Lee, and J. S. Watson, "A Solubility Model for Aqueous Solutions Containing Sodium, Fluoride, and Phosphate Ions," *Ind. Eng. Chem. Res.* **39**, 518–26 (2000).
42. R. D. Hunt et al., *Waste Preparation and Transport Chemistry: Results of the FY2000 Studies*, ORNL/TM-2000/298, UT Battelle, LLC, Oak Ridge National Laboratory (2000).
43. D. T. Hobbs and D. G. Karraker, "Recent Results on the Solubility of Uranium and Plutonium in Savannah River Waste Supernate," *Nucl. Technol.* **114**, 318–24 (1996); K. H. Gayer and H. Leider, "The Solubility of Uranium Trioxide, $UO_3 \cdot H_2O$, in Solutions of Sodium Hydroxide and Perchloric Acid at 25°," *J. Am. Chem. Soc.* **77**, 1448–50 (1955).
44. B. Toghiani, J. S. Linder, C. F. Weber, and R. D. Hunt, *Modeling of Sulfate Double-Salt in Nuclear Wastes*, ORNL/TM-2000/317, UT-Battelle, LLC, Oak Ridge National Laboratory (2000).
45. C. F. Weber and E. C. Beahm, *Chemical Modeling of Waste Sludges*, ORNL/TM-13200, Lockheed Martin Energy Research Corp., Oak Ridge National Laboratory (1996).
46. J. C. Peiper and K. S. Pitzer, "Thermodynamics of Aqueous Carbonate Solutions Including Mixtures of Sodium Carbonate, Bicarbonate, and Chloride," *J. Chem. Thermodyn*. **14**, 613 (1982).

APPENDIX A

Table A.1. Coefficients for Gibbs Energy of Formation

$\mu^0/RT = A + B\,(T - T_0) + C\,(1/T_0 - 1/T) + D\,\ln(T/T_0) + E\,(T^2 - T_0^2)$

	A	B	C	D	E	Ref.[a]
Ar	0	0	0	0	0	
H_2O	-95.667	0	35520.58	-3.82631	0	38
Na^+	-105.642	0	29203.98	-1.16439	0	38
K^+	-113.968	0	29220.3	3.731026	0	38
H^+	0	0	0	0	0	
UO_2^{2+}	-384.629	0	131094.3	-28.2168	0	38
NO_3^-	-44.707	0	20337.25	15.17588	0	38
OH^-	-63.446	0	21972.73	19.03521	0	38
Cl^-	-52.951	0	14731.27	17.92967	0	38
F^-	-113.643	0	35464.6	16.25967	0	38
PO_4^{3-}	-410.766	0	132983.5	69.11808	0	38
HPO_4^{2-}	-439.166	0	174154.1	-60.0832	0	39
NO_2^-	-12.931	0	7624.179	16.5833	0	38
$Al(OH)_4^-$	-526.779	0	180307.3	0.842528	0	7
CO_3^{2-}	-212.960	0	68841.02	41.36688	0	38
HCO_3^-	-236.246	0	80160.2	9.67583	0	40
SO_4^{2-}	-300.285	0	96620.31	42.66527	0	38
Si(1,1)	-505.064	0	161966.7	0	0	
Si(2,1)	-458.242	0	131188	0	0	
Si(2,2)	-450.841	0	141043.4	0	0	
Si(4,2)	-421.193	0	120657.6	0	0	
Si(6,3)	-382.663	0	131398.4	0	0	
Si(2,4)	-417.759	0	135166.3	0	0	
Si(4,4)	-407.813	0	126749.7	0	0	
Si(6,6)	-359.192	0	109394.7	0	0	
Si(4,8)	-357.764	0	110000	0	0	
Si(8,8)	-357.379	0	107550.4	0	0	
$C_2O_4^{2-}$	-271.956	0	81933.21	57.9329	0	38
Si(0,1)	-527.652	0	180643.6	-16.778	0	38
$Al(OH)_3$	-465.971	0	155087.8	1.583907	0	38
$NaNO_3$	-147.822	0	61480.8	-19.1222	0	
$NaNO_2$	-114.658	0	42970.1	0	0	
$Na_2CO_3 \cdot H_2O$	-518.372	0	168431.7	0	0	
$Na_2CO_3 \cdot 7H_2O$	-1094.799	0	387532.6	0	0	
$Na_2CO_3 \cdot 10H_2O$	-1382.743	0	493460.2	0	0	
KNO_3	-158.891	0	0	0	0	
NaCl	-155.030	1.198614	0	0	-0.0012	
KCl	-164.878	0	0	0	0	

Table A.1 (continued)

	A	B	C	D	E	Ref.
NaF	-219.391	2.022907	0	0	-0.00209	41
$Na_3PO_4 \cdot 12H_2O \cdot {}^1/_4NaOH$	-1926.923	-1351	-4.2E+07	415570.9	0.731171	39
$Na_2HPO_4 \cdot 12H_2O$	-1803.470	7.65392	0	0	0	39
$2Na_3PO_4 \cdot NaF \cdot 19H_2O$	-3512.445	36.15256	0	0	-0.03774	41
$UO_2(OH)_2$	532.673	5.422982	0	0	-0.00561	42
$Na_2U_2O_7$	-1113.060	11.34351	0	0	-0.01175	43
SiO_2(am)	-342.486	0	112091.7	-11.4904	0	
OH-sodalite	-5350.580		1547994	-191.791		
NO_3-Cancrinite	-5454.573	0	1465869	0	0	
$K_2C_2O_4 \cdot W$	-596.677	0	172341.5	82.73543	0	9
$Na_2C_2O_4$	-488.595	0	157821.3	21.23335	0	9
Na_2SO_4	-513.057	4.78648	0	0	-0.0049	44
$Na_2SO_4 \cdot 10H_2O$	-1472.023	15.5281	0	0	-0.01624	44
$Na_2SO_4 \cdot NaNO_3 \cdot 2H_2O$	-852.691	8.84139	0	0	-0.00932	44

[a] Omission of reference number indicates values were determined in the course of this study.

Table A.2. Binary Pitzer Parameters

Ionic species		Parameter	A	B	C	D	Temp.	Ref
Na^+	NO_3^-	$\beta^{(0)}$	0.00204	0	406.5	-1.04	0–100	
Na^+	NO_3^-	$\beta^{(1)}$	0.2368	0	712.4	-1.214		
Na^+	NO_3^-	C	0.00008	0	-27.22	0.0756		
Na^+	OH^-	$\beta^{(0)}$	0.0869	0	356.02	-1.0814	0–150	6
Na^+	OH^-	$\beta^{(1)}$	0.2481	0	-173.16	1.2073		6
Na^+	OH^-	C	0.0039	0	-34.22	0.0842		6
Na^+	Cl^-	$\beta^{(0)}$	0.0743	0	283.52	-0.7325	0–150	6
Na^+	Cl^-	$\beta^{(1)}$	0.2744	0	-15.68	0.3162		6
Na^+	Cl^-	C	0.0008	0	-15.47	0.0354		6
Na^+	F^-	$\beta^{(0)}$	0.033	0	246.8	-0.6728	0–100	41
Na^+	F^-	$\beta^{(1)}$	0.2456	0	2833	-9.451		41
Na^+	F^-	C	0.00281	0	12.25	-0.0436		41
Na^+	PO_4^{3-}	$\beta^{(0)}$	0.2534	0	130.3	0.1247	0–100	39
Na^+	PO_4^{3-}	$\beta^{(1)}$	3.7384	0	23420	-70.37		39
Na^+	PO_4^{3-}	C	-0.0226	0	0	-0.00016		39
Na^+	HPO_4^{2-}	$\beta^{(0)}$	-0.03045	0	1826	-5.159	0–100	39
Na^+	HPO_4^{2-}	$\beta^{(1)}$	1.3504	0	6023	-18.77		39
Na^+	HPO_4^{2-}	C	0.00359	0	-282.6	0.8267		39
Na^+	NO_2^-	$\beta^{(0)}$	0.0498	0	-165.6	0.5931	25–100	9
Na^+	NO_2^-	$\beta^{(1)}$	0.2177	0	3124	-8.621		9
Na^+	NO_2^-	C	-0.0012	0	10.71	-0.0364		9
Na^+	$Al(OH)_4^-$	$\beta^{(0)}$	0.0513	0	356.02	-1.0814	0–100	7
Na^+	$Al(OH)_4^-$	$\beta^{(1)}$	0.2481	0	-173.16	1.2073		7
Na^+	$Al(OH)_4^-$	C	0.0013	0	-34.22	0.0842		7
Na^+	CO_3^{2-}	$\beta^{(0)}$	0.0362	-0.0233	-1108.38	11.19856	0–90	40
Na^+	CO_3^{2-}	$\beta^{(1)}$	1.51	-0.09989	-4412.51	44.58207		40
Na^+	CO_3^{2-}	C	0.00184					40
Na^+	HCO_3^-	$\beta^{(0)}$	0.028	-0.01446	-682.886	6.899586	0–90	40
Na+	HCO_3^-	$\beta^{(1)}$	0.044	-0.02447	-1129.39	11.41086		40
Na^+	SO_4^{2-}	$\beta^{(0)}$	0.0262	0	570.6	-1.3547	25–130	44
Na^+	SO_4^{2-}	$\beta^{(1)}$	1.0277	0	-85.69	2.017		44
Na^+	SO_4^{2-}	C	0.00126	0	-35.37	0.0811		44
Na^+	$C_2O_4^{2-}$	$\beta^{(0)}$	0.1621	0	-1452		0–110	9
Na^+	$C_2O_4^{2-}$	$\beta^{(1)}$	1.4533	0	16676			9

Table A.2 (continued)

Ionic Strength		Parameter	A	B	C	D	Temp.	Ref.
Na^+	$C_2O_4^{2-}$	C	-0.0822	0	142			9
Na^+	Si(1,1)	$\beta^{(0)}$	-2.2564		-1838		20–102	
Na^+	Si(1,1)	$\beta^{(1)}$	10.7265					
Na^+	Si(1,1)	C	0.2744					
Na^+	Si(2,1)	$\beta^{(0)}$	0.9477		67.23		20–102	
Na^+	Si(2,1)	$\beta^{(1)}$	-27.1254					
Na^+	Si(2,1)	C	-0.0915					
Na^+	Si(2,2)	$\beta^{(0)}$	-0.1343		-1092		20–102	
Na^+	Si(2,2)	$\beta^{(1)}$	-7.6464					
Na^+	Si(2,2)	C	-0.0043					
Na^+	Si(4,2)	$\beta^{(0)}$	0.2362		-265.1		20–102	
Na^+	Si(4,2)	$\beta^{(1)}$	-11.6927					
Na^+	Si(4,2)	C	-0.0136					
Na^+	Si(6,3)	$\beta^{(0)}$	0.3825		-2029		20–102	
Na^+	Si(6,3)	$\beta^{(1)}$	1.1225					
Na^+	Si(6,3)	C	-0.0293					
Na^+	Si(2,4)	$\beta^{(0)}$	-0.4831		-1159		20–102	
Na^+	Si(2,4)	$\beta^{(1)}$	-3.82					
Na^+	Si(2,4)	C	0.0218					
Na^+	Si(4,4)	$\beta^{(0)}$	-0.347		-1548		20–102	
Na^+	Si(4,4)	$\beta^{(1)}$	-1.6082					
Na^+	Si(4,4)	C	0.0083					
Na^+	Si(6,6)	$\beta^{(0)}$	-0.4626		-1580		20–102	
Na^+	Si(6,6)	$\beta^{(1)}$	-0.9638					
Na^+	Si(6,6)	C	0.0167					
Na^+	Si(4,8)	$\beta^{(0)}$	-2.7046		0		20–102	
Na^+	Si(4,8)	$\beta^{(1)}$	6.2351					
Na^+	Si(4,8)	C	0.1148					
Na^+	Si(8,8)	$\beta^{(0)}$	0.0031		-121.9		20–102	
Na^+	Si(8,8)	$\beta^{(1)}$	-8.3161					
Na^+	Si(8,8)	C	-0.0089					
K^+	NO_3^-	$\beta^{(0)}$	-0.0806	0	428.7	-0.9718	0–100	
K^+	NO_3^-	$\beta^{(1)}$	0.0764	0	1362	-2.698		
K^+	NO_3^-	C	0.0025	0	-24.3	0.0619		
K^+	OH^-	$\beta^{(0)}$	0.1632	0	-567.6	1.77	0–100	
K^+	OH^-	$\beta^{(1)}$	0.097	0	9256	-29.83		
K^+	OH^-	C	-0.0007	0	25.54	-0.0864		
K^+	Cl^-	$\beta^{(0)}$	0.0475	0	191.98	-0.4764	0–150	9
K^+	Cl^-	$\beta^{(1)}$	0.2148	0	46.73	0.2695		9
K^+	Cl^-	C	-0.0003	0	137.72	-0.6513		9
K^+	F^-	$\beta^{(0)}$	0.08089					9
K^+	F^-	$\beta^{(1)}$	0.2021					9

Table A.2 (continued)

Ionic Strength		Parameter	A	B	C	D	Temp.	Ref.
K^+	F^-	C	0.00046					6
K^+	PO_4^{3-}	$\beta^{(0)}$	0.2585					6
K^+	PO_4^{3-}	$\beta^{(1)}$	4.316					6
K^+	PO_4^{3-}	C	-0.00029					6
K^+	HPO_4^{2-}	$\beta^{(0)}$	0.0248					6
K^+	HPO_4^{2-}	$\beta^{(1)}$	1.2743					6
K+	HPO_4^{2-}	C	0.0058					6
K^+	NO_2^-	$\beta^{(0)}$	0.0128	0	-339.2	-0.8802	0–100	9
K^+	NO_2^-	$\beta^{(1)}$	0.0668	0	37818	-113.6		9
K^+	NO_2^-	C	-0.0005	0	-6.567	0.01522		9
K^+	$Al(OH)_4^-$	$\beta^{(0)}$	0.1276	0	-567.6	1.77	0–100	7
K^+	$Al(OH)_4^-$	$\beta^{(1)}$	0.097	0	9256	-29.83		7
K^+	$Al(OH)_4^-$	C	-0.006	0	25.54	-0.0864		7
K^+	CO_3^{2-}	$\beta^{(0)}$	0.1288	0.0011	-1.81E-05	0	0–90	40
K^+	CO_3^{2-}	$\beta^{(1)}$	1.433	0.00436	-0.00119	0		40
K^+	CO_3^{2-}	C	-0.00018	0	0	0		40
K^+	HCO_3^-	$\beta^{(0)}$	-0.01071	0.001	0.000699	-4.70E-06	0–90	40
K^+	HCO_3^-	$\beta^{(1)}$	0.0478	0.0011	-0.00094	6.16E-06		40
K^+	$C_2O_4^{2-}$	$\beta^{(0)}$	0.0643		85.52		0–108	9
K^+	$C_2O_4^{2-}$	$\beta^{(1)}$	1.5235		650.2			9
K^+	$C_2O_4^{2-}$	C	0.0005		-3.712			9
H^+	NO_3^-	$\beta^{(0)}$	0.1168					6
H^+	NO_3^-	$\beta^{(1)}$	0.3546					6
H^+	NO_3^-	C	-0.0027					6
H^+	Cl^-	$\beta^{(0)}$	0.1769					6
H^+	Cl^-	$\beta^{(1)}$	0.2973					6
H^+	Cl^-	C	0.000362					6
UO_2^{2+}	NO_3^-	$\beta^{(0)}$	0.4607					6
UO_2^{2+}	NO_3^-	$\beta^{(1)}$	1.6133					6
UO_2^{2+}	NO_3^-	C	-0.01115					6
UO_2^{2+}	OH^-	$\beta^{(0)}$	0.4274					6

Table A.2 (continued)

Ionic Strength		Parameter	A	B	C	D	Temp.	Ref.
UO_2^{2+}	OH^-	$\beta^{(1)}$	1.644					6
UO_2^{2+}	OH^-	C	-0.01303					6
UO_2^{2+}	Cl^-	$\beta^{(0)}$	0.4607					6
UO_2^{2+}	Cl^-	$\beta^{(1)}$	1.6133					6
UO_2^{2+}	Cl^-	C	-0.01115					6
UO_2^{2+}	CO_3^{2-}	$\beta^{(0)}$	0.4607					6
UO_2^{2+}	CO_3^{2-}	$\beta^{(1)}$	1.6133					6
UO_2^{2+}	CO_3^{2-}	C	-0.01115					6
UO_2^{2+}	HCO_3^-	$\beta^{(0)}$	0.322					6
UO_2^{2+}	HCO_3^-	$\beta^{(1)}$	1.827					6
UO_2^{2+}	HCO_3^-	C	-0.0176					6

Table A.3. Ternary Pitzer Parameters

Ionic species			Parameter	A	C	Temp.	Ref.
NO_3^-	OH^-		θ	-0.0547			45
NO_3^-	Cl^-		θ	0.016			6
NO_3^-	$Al(OH)_4^-$		θ	-0.0272			7
NO_3^-	SO_4^{2-}		θ	0.0673			44
NO_3^-	$C_2O_4^{2-}$		θ	-0.1093		15–75	9
OH^-	Cl^-		θ	-0.05			6
OH^-	F^-		θ	0.1193			41
OH^-	PO_4^{3-}		θ	0.1			39
OH^-	CO_3^{2-}		θ	-0.1632			6
OH^-	SO_4^{2-}		θ	-0.013			6
OH^-	$Al(OH)_4^-$		θ	0.014			7
OH^-	$C_2O_4^{2-}$		θ	-0.1118		0–108	9
Cl^-	F^-		θ	-0.01			41
Cl^-	PO_4^{3-}		θ	0.2559			39
NO_2^-	$Al(OH)_4^-$		θ	0.00197			9
Cl^-	CO_3^{2-}		θ	-0.053			46
Cl^-	HCO_3^-		θ	0.036			46
Cl^-	SO_4^{2-}		θ	0.03			6
F^-	PO_4^{3-}		θ	0.55			41
PO_4^{3-}	NO_2^-		θ	0.1047			
CO_3^{2-}	HCO_3^-		θ	0.09			6
CO_3^{2-}	SO_4^{2-}		θ	0.02			6
HCO_3^-	SO_4^{2-}		θ	0.01			6
Na^+	K^+	NO_3^-	Ψ	-0.006			45
Na^+	K^+	OH^-	Ψ	0.004			45
Na^+	K^+	Cl^-	Ψ	-0.0018			6
Na^+	K^+	CO_3^{2-}	Ψ	0.003			6
Na^+	K^+	HCO_3^-	Ψ	-0.003			6
Na^+	K^+	SO_4^{2-}	Ψ	-0.01			6
Na^+	H^+	NO_3^-	Ψ	-0.00274			45
Na^+	H^+	Cl^-	Ψ	-0.004			6
Na^+	UO_2^{2+}	NO_3^-	Ψ	0.3879			

Table A.3 (continued)

Ionic Species			Parameter	A	C	Temp.	Ref.
Na^+	UO_2^{2+}	OH^-	Ψ	-0.2556			
Na^+	NO_3^-	OH^-	Ψ	0.0002			45
Na^+	NO_3^-	Cl^-	Ψ	-0.006			45
Na^+	NO_3^-	$Al(OH)_4^-$	Ψ	0.0047			
Na^+	NO_3^-	SO_4^{2-}	Ψ	0.00335			44
Na^+	NO_3^-	$C_2O_4^{2-}$	Ψ	0.1895	-95.66	15–75	9
Na^+	OH^-	Cl^-	Ψ	-0.0063			6
Na^+	OH^-	F^-	Ψ	-0.035			41
Na^+	OH^-	PO_4^{3-}	Ψ	0.03			39
Na^+	OH^-	CO_3^{2-}	Ψ	0.0172			6
Na^+	OH^-	SO_4^{2-}	Ψ	-0.009			6
Na^+	OH^-	$Al(OH)_4^-$	Ψ	-0.0048			7
Na^+	OH^-	$C_2O_4^{2-}$	Ψ	0.1		0–108	9
Na^+	Cl^-	F^-	Ψ	-0.00218			41
Na^+	Cl^-	PO_4^{3-}	Ψ	0			39
Na^+	Cl^-	CO_3^{2-}	Ψ	0.0085			6
Na^+	Cl^-	HCO_3^-	Ψ	-0.015			6
Na^+	Cl^-	SO_4^{2-}	Ψ	0			6
Na^+	F^-	PO_4^{3-}	Ψ	0			41
Na^+	F^-	HPO_4^2	Ψ	0			41
Na^+	PO_4^{3-}	NO_2^-	Ψ	0.0537			
Na^+	CO_3^{2-}	HCO_3^-	Ψ	0.002			6
Na^+	CO_3^{2-}	SO_4^{2-}	Ψ	-0.005			6
Na^+	HCO_3^-	SO_4^{2-}	Ψ	-0.005			6
Na^+	NO_2^-	$Al(OH)_4^-$	Ψ	0.0054			
Na^+	NO_2^-	$C_2O_4^{2-}$	Ψ	0.23			
K^+	H+	NO_3^-	Ψ	-0.0103			45
K^+	H^+	Cl^-	Ψ	-0.011			45
K+	NO_3^-	OH^-	Ψ	-0.0032			45
K^+	NO_3^-	Cl^-	Ψ	-0.0031			45
K^+	OH^-	Cl^-	Ψ	-0.0032			45
K^+	OH^-	CO_3^{2-}	Ψ	-0.01			6

Table A.3 (continued)

Ionic Species			Parameter	A	C	Temp.	Ref.
K^+	OH^-	SO_4^{2-}	Ψ	-0.05			6
K^+	OH^-	$C_2O_4^{2-}$	Ψ	0.005		0–108	9
K^+	Cl^-	F^-	Ψ	-0.0135			41
K^+	Cl^-	CO_3^{2-}	Ψ	0.004			6
K^+	Cl^-	HCO_3^-	Ψ	-0.015			6
K^+	Cl^-	SO_4^{2-}	Ψ	-0.005			6
K^+	CO_3^{2-}	SO_4^{2-}	Ψ	-0.009			6
K^+	HCO_3^-	SO_4^{2-}	Ψ	0.005			6
Na^+	Si(0,1)		λ	0			
NO_3^-	Si(0,1)		λ	0.0563			
Cl^-	Si(0,1)		λ	0.0478			
K^+	Si(0,1)		λ	-0.0504			

APPENDIX B

ESTIMATION OF ΔS°_{298} AND ΔG°_{T} FOR CANCRINITE

APPENDIX B

ESTIMATION OF ΔS°_{298} AND ΔG°_{T} FOR CANCRINITE[†]

The table below lists a comparison of the standard entropy change of formation at 298 K for 10 aluminosilicates with values obtained from summing the standard entropy changes for the component oxides. The comparison shows that ΔS°_{298} obtained from the sum of the oxides is a reasonably good estimate of listed values. All entropy changes were taken from Ref. 38.

For cancrinite as:

$$Na_{7.68}(Al_6Si_6O_{24})(NO_3)_{1.68}(H_2O)_{4.1},$$

summation of ΔS°_{298} from Na_2O, SiO_2, Al_2O_3, $NaNO_3$, and H_2O gives ΔS°_{298} = −875.14 cal/K· mole. The summation of ΔS°_{298} from $NaAlSiO_4$, $NaNO_3$, and H_2O is −846.68 cal/K · mole. We use the average of these values: −860.91 ± 14.23 cal/K · mole.

Table B.1. Comparison of listed values[a] for ΔS°_{298} with those obtained by summing oxides

Species	ΔS°_{298} (cal/K · mole)		$\frac{\Delta S^{\circ}_{298}(\text{Sum})}{\Delta S^{\circ}_{298}(\text{Listed})} \times 100$
	Sum of oxides	Listed	
$NaAlSiO_4$	−96.652	−91.908	105.16
$Na_2O{\cdot}Al_2O_3{\cdot}2SiO_2$	−193.303	−183.839	105.15
$Na_2O{\cdot}Al_2O{\cdot}4SiO_2$	−280.541	−286.490	97.92
$Na_2O{\cdot}Al_2O_3$	−106.065	−102.374	103.61
$Na_2O{\cdot}SiO_2$	−74.796	−74.450	100.46
$Na_2O{\cdot}2SiO_2$	−118.415	−116.959	101.24
$2Na_2O{\cdot}SiO_2$	−105.973	−104.993	100.93
$NaAlSi_2O_6{\cdot}H_2O$	−179.301	−180.723	99.21
$Al_2O_3{\cdot}2SiO_2{\cdot}2H_2O$	−240.186	−256.617	93.60
$Na_{.96}Al_{.96}Si_{2.04}O_6{\cdot}H_2O$	−178.924	−176.111	101.60

[a] Listed values obtained from ref. 38.

[†]Analysis by E. C. Beahm, now retired from ORNL.

Gibbs energy of formation is defined as:

$$\Delta G^\circ = \Delta H^\circ - T\,\Delta S^\circ$$

where T is temperature (K). A value of ΔH°_{298} was taken from ref. 28; together with the entropy value mentioned above, a reasonable estimate is

$$\Delta G^\circ_{298} = -3{,}231.42 \pm 6.8 \text{ kcal/mol} = -5454.573 \text{ kJ/mol}.$$

APPENDIX C

SWPF FEED COMPOSITIONS

APPENDIX C

SWPF FEED COMPOSITIONS†

Table C.1 Feed compositions

Component	Year 1	Year 2	Year 3	Year 4	Year 5	Year 6	Year 7	Year 8	Year 9	Year 10	Year 11	Year 12	Year 13
H_2O, wt %	65.6	67.0	65.8	66.1	68.1	67.2	65.6	67.7	65.8	68.6	70.0	69.5	77.8
$NaNO_3$, wt %	19.4	15.2	19.1	19.1	13.4	16.6	19.8	14.1	19.8	17.1	14.0	14.5	9.77
NaOH, wt %	5.78	7.42	5.34	5.07	8.80	7.58	5.44	8.51	6.12	5.79	6.69	6.32	5.46
$NaNO_2$, wt %	2.39	4.33	2.62	2.69	4.21	2.70	1.97	4.29	1.36	2.07	3.82	3.87	2.53
$NaAlO_2$, wt %	1.92	2.26	2.24	2.22	2.51	2.14	2.02	1.90	1.99	1.75	2.09	2.19	1.54
Na_2SO_4, wt %	2.24	1.46	2.39	2.43	1.07	1.58	2.47	1.45	2.61	2.24	1.48	1.54	1.18
Na_2CO_3, wt %	1.84	1.42	1.48	1.41	1.15	1.54	1.80	1.23	1.51	1.66	0.98	1.23	1.23
Other salts, wt %	0.68	0.81	0.87	0.85	0.60	0.56	0.71	0.69	0.69	0.61	0.77	0.74	0.41
KOH, wt %	0.063	0.066	0.048	0.053	0.115	0.102	0.071	0.097	0.094	0.085	0.059	0.048	0.054
NH_4NO_3, wt %	1.5E-04	6.1E-03	3.7E-03	3.4E-03	4.2E-03	4.9E-04	5.0E-04	4.4E-02	5.3E-03	3.6E-04	6.5E-03	6.3E-03	1.5E-03
CsOH, wt %	1.3E-03	1.4E-03	9.6E-04	9.2E-04	2.1E-03	2.1E-03	1.6E-03	1.3E-03	8.7E-04	2.7E-03	2.3E-03	2.2E-03	3.7E-03
$Na_2U_2O_7$, wt %	0.013	3.4E-03	1.8E-02	1.3E-04	7.6E-04	6.9E-02	1.3E-04	0.042	6.5E-06	2.4E-03	8.1E-03	1.1E-03	3.4E-03
$Sr(OH)_2$, wt %	trace	trace	trace	trace	trace	trace	trace	trace	trace	trace	trace	trace	trace
sludge, wt %	0.062	0.060	0.078	0.079	0.040	0.040	0.066	0.054	0.070	0.053	0.063	0.061	0.025
HgO, wt %	2.1E-03	2.0E-03	1.6E-03	1.6E-03	3.4E-03	4.0E-03	1.4E-03	3.5E-03	1.2E-03	1.9E-03	2.2E-03	2.3E-03	2.8E-03
Total, wt %	100.0	100.0	100.0	100.0	100.0	100.0	100.0	100.0	100.0	100.0	100.0	100.0	100.0
Density, Kg/L	1.294	1.283	1.308	1.299	1.274	1.279	1.301	1.268	1.301	1.263	1.259	1.263	1.181
[Na+], M	6.43	6.44	6.35	6.21	6.43	6.40	6.39	6.43	6.43	5.81	5.69	5.76	4.09
[K+], M	0.015	0.015	0.011	0.012	0.026	0.023	0.017	0.022	0.022	0.019	0.013	0.011	0.011
[Hg], mg/L	26	24	19	19	40	48	16	41	14	23	26	27	30

†Taken from ref. 35.

INTERNAL DISTRIBUTION

1. W. C. Carter, 6011, MS-6370
2. M. B. Emmett, 6011, MS-6370
3. R. D. Hunt, 4500N, MS-6223
4. R. T. Jubin, 4501, MS-6223
5. T. E. Kent, 4501, MS-6223
6. M. A. Kuliasha, 6025, MS-6435
7. A. J. Mattus, 4501, MS-6221
8. C. P. McGinnis, 4500N, MS-6176
9. C. V. Parks, 6011, MS-6370
10. P. A. Taylor, 4501, MS-6221

11–14. C. F. Weber, 6011, MS-6370

15. ORNL Laboratory Records
    4500N, MS-6254
16. Central Research Library
    4500N, MS-6191

EXTERNAL DISTRIBUTION

17. J. T. Carter, Westinghouse Savannah River Company, P.O. Box 616, Bldg. 704-3N, Room S151, Aiken, SC 29808
18. C. F. Jove Colon, Sandia National Laboratory, P.O. Box 5800 / MS 0750, Albuquerque, NM 87185-0750
19. S. D. Fink, Westinghouse Savannah River Co., P.O. Box 616, Bldg. 773-A, Room B112, Aiken, SC 29808
20. F. F. Fondeur, Westinghouse Savannah River Co., P.O. Box 616, Bldg.773A, Aiken, SC 29808
21. M. W. Geeting, Westinghouse Savannah River Co., P.O. Box 616, Bldg.704-196N, Room S411, Aiken, SC 29808
22. H. D. Harmon, Tank Focus Area Salt Processing Program, P.O. Box 616, Bldg. 704-3N, Room S151, Aiken, SC 29808
23. D. T. Hobbs, Westinghouse Savannah River Co., P.O. Box 616, Bldg.773A, Aiken, SC 29808
24. R. A. Jacobs, Westinghouse Savannah River Co., P.O. Box 616, Bldg. 704-3N, Room S252, Aiken, SC 29808
25. D. M. Jantzen, Westinghouse Savannah River Co., P.O. Box 616, Bldg.773A, Aiken, SC 29808
26. J. L. Krumhansl, Sandia National Laboratory, P.O. Box 5800 / MS 0750, Albuquerque, NM 87185-0750
27. D. J. McCabe, Westinghouse Savannah River Co., P.O. Box 616, Bldg.773A, Aiken, SC 29808

28–29. Office of Scientific and Technical Information, U.S. Department of Energy, P.O. Box 62, Oak Ridge, TN 37831

30. J. A. Pike, Westinghouse Savannah River Co., P.O. Box 616, 704-3N, Room S151, Aiken, SC 29808
31. S. N. Schlahta, Tank Focus Area Salt Processing Program, P.O. Box 616, 704-3N, Room S151, Aiken, SC 29808
32. D. D. Walker, Westinghouse Savannah River Co., P.O. Box 616, Bldg.773A, Room G-124, Aiken, SC 29808
33. D. W. Wester, Pacific Northwest National Laboratory, P.O. Box 999 / MS P7-25, Richland, WA 99352
34. W. R. Wilmarth, Westinghouse Savannah River Co., P.O. Box 616, Bldg.773A, Aiken, SC 29808